Reviewer #1

I appreciate the efforts undertaken by the authors to revise the manuscript and respond to the reviewers' concerns. Although the paper has gone under major revisions, some of my concerns from before are still not fully addressed. I therefore cannot accept the manuscript and suggest major revisions. Personally, I believe it's a pity that the full extent of the chemical analysis results are not presented along with the optical properties of the aerosols since explanation of the optical properties is highly dependent on the chemical nature of the aerosols. I strongly encourage the authors to combine the two papers together. Please see below my comments:

Author's response:

We thank the reviewer for the earlier very constructive comments that helped improve the paper and the current comments will surely improve the paper further. With respect to combining the papers describing the optical and chemical properties, the authors initially considered that and felt the paper would be too long and too complicated, and decided to present it in two parts. The review process on part 2 is almost complete and the comments provided are positive. It is very likely that the second part will be published about the same time as part 1if accepted.

From our perspective as authors, we considered both papers as different aspects of a whole work. However, we did not fully appreciate the perspective of the reader, since it would be hardly fair to expect them to read both papers to understand one of them alone. As such, we thank the reviewer for their insight on this matter. As a result, we have added more results of the chemical analysis in this paper and provided several figures and tables in the supplementary documentation as discussed below in response to each comment. This additional material is not simply copied from Part 2, but tailored to the work in question.

Note also the line numbers used by the reviewer refer to the line numbers on the marked up (track change) version. we will be using the line numbers of the clean copy.

General Reviewer Comments:

- Discussion on the contribution of multiply charged particles is still confusing and not consistent; the authors first indicate that the error is not significant for 300 nm and 400 nm particles considered in this work; then they explain the procedure using an APM and conclude that the error in SSA for fresh 200 nm and 300 nm particles is ~8%. In the next paragraph, they indicate the error is more significant for the flaming conditions, but do not indicate if the 8% estimate includes flaming aerosols and if not, what the error for such conditions are. This discussion still needs to be cleared up and be consistent and complete for all sizes and conditions considered here.

Authors Response:

We thank the reviewer for the constructive comments. We rewrote both paragraphs (lines 355-372) and described in detail the issue of multiply charged particles and Mie theory calculation.

Changes made in the manuscript

"Submicron aerosol show size-dependent SSA values in visible wavelengths. Size-selected SSA values measured at 532 nm in this study are compared with the size selected SSA values calculated using Mie theory for two different refractive indices, as shown in Figure 3. These refractive indices were proposed by Bond and Bergstrom (2006) for BC and Levin et al. (2010) for smoldering biomass burning particles. While no pronounced size dependence was observed for aerosol from flaming-dominated combustion, contrary to what was predicted by Mie theory, the SSA does show size dependence for aerosol from smoldering-dominated combustion. This is due to the impact of multiply charged aerosol not discriminated by the DMA. Since we did not correct for the presence of multiply charged particles in this work, as described in section 2.5, this behavior was expected. The impact of multiply charged particles is more significant for flaming-dominated combustion (no pronounced size-dependent SSA) compared with the smoldering-dominated combustion (with some size-dependent SSA). This is a consequence of difference in particle size distributions. As shown in **Figure S3**, the presence of a second peak in the size distribution for flaming-dominated burns was expected to increase the impact of multiply charged particles on the observed.

Recently, we estimated the impact of multiply charged particles on SSA using an Aerosol Particle Mass Analyzer (APM; Kanomax model 3602). We didn't have this capability early in this study. APM was connected in-line after the DMA and subsequent optical properties were measured for freshly emitted aerosol. Details about the measurement strategy is given by Radney and Zangmeister (2016). It was found that, for smoldering-dominated burns, our SSA values were over estimated by a maximum of 8% for 200 and 300 nm sizes and by 5% for 400 nm size particles. Whereas, for flaming-dominated burns, our SSA values were overestimated by 12% for 200 and 300 nm sizes and by 9% for 400 nm size.

Reviewer comment

- The increase in temperature during the first hour of aging is significant and will impact partitioning of the semivolatile components. This effect needs to be discussed.

Author's response

We agree with the reviewer that the increase in temperature impacts partitioning of semivolatile compounds. The particle/gas partition coefficient, Kp is temperature dependent (Pankow, 1987) and its value is needed to predict the unknown gas-phase SVOC concentration from its measured concentration in airborne particles. However, Kp values can only be retrieved from the literature for a limited number of SVOCs. Furthermore, for SVOCs, the time to reach equilibrium partitioning between gas-phase and airborne particles varies between seconds to days depending on the volatility of the SVOCs and the diameter of the particle (Weschler and Nazaroff, 2008;Wei et al., 2016)). Ranjan et al. (2012) studied the gas–particle partitioning from POA emissions from diesel engines and showed that the results vary by about a factor of 4 across the atmospherically relevant range of temperature and organic aerosol concentrations confirming the semivolatile nature of POA emissions.

We did not measure the partitioning of the semivolatile components in this work. It is possible that this may impact the optical properties measurements following photochemical aging. The changes in optical properties could be attributed to be in part because of this.

Changes made in the manuscript:

We will include the discussion below on the partitioning of the semivolatile components due to temperature increase during photochemical aging qualitatively in section 2.2

"The temperature increase during photochemical aging can impact partitioning of the semivolatile components. The gas phase partitioning coefficient is temperature dependent though its value is only available for a limited number of semivolatile compounds. We did not measure the impact of temperature on partitioning of the semivolatile components, but it is possible that the observed change in optical properties during photochemical aging could in part be attributed to this effect."

Reviewer comment

Regarding the Mie calculations…. It seems the authors just calculated scattering and absorption (or extinction) cross sections of the aerosols, assuming an overall RI based on RI of BC and bulk aerosol from Levin et al. In that case, what was the overall RI that includes contributions of BC and other components of the freshly emitted aerosols and how was this RI estimated? In other words, if RI of BC is combined with another RI, what weighting factor is given to BC vs. other aerosol components. The text should also clearly demonstrate that an inherent assumption here is that aerosols are internally mixed at all sizes such that the bulk estimate of RI is the same for all sizes. A discussion on how good such an assumption is (or is not) should also be provided.

Author Response

We are sorry for the confusion about the SSA calculation using Mie theory. We will provide a more detailed explanation:

- *In Figure 3, the symbols (square, diamond and circle) are the estimated SSA values from this study based on the size-dependent scattering and extinction measurements.*
- *We calculated the size dependent SSA for refractive index 1.95- i 0.79 using Mie theory (Black line in Figure 3).*
- *We calculated the size dependent SSA for refractive index 1.6 - i 0.1 using Mie theory (Red line in Figure 3).*

Since we are not combining RI of BC and bulk aerosol, there is no need for making any assumption on mixing state, weighting factor, etc. We used Mie theory twice for the two different cases to calculate the SSA for two different values of the refractive index.

Changes made in the manuscript

As stated above the following sentence will be added in the manuscript to clarify this point

"Submicron aerosol show size-dependent SSA values in the visible wavelength range. Size-selected SSA values measured at 532 nm in this study are compared with the size-selected SSA values calculated using Mie theory for two different refractive indices, as shown in Figure 3. These refractive indices were proposed by Bond and Bergstrom, (2006) for BC and Levin et al. (2010) for aerosol produced in smoldering biomass burning."

Reviewer comment

- Effect of NOx on SOA from aromatics: although NOx data are not available for these experiments, I think the authors should indicate that if NOx concentrations were high, it's possible

that yields from the injected aromatics were very small and that can explain why there wasn't any change in the photochemical aging results with and without VOCs. This is important to highlight before hypothesizing that anthropogenic pollution doesn't affect BB aerosol optical properties.

Author Response: *We thank the reviewer for this suggestion. This will be addressed, as follows in section 3.5.*

Changes made in the manuscript

"While it is possible that the relatively long aging time could obscure some of the effects due to the presence of VOCs, it is also possible that molecular species are dominated by combustion products, and the effects of additional VOCs are insignificant. The later would suggest that the three-aromatic species representing anthropogenic pollutants do not seem to affect the optical properties of BB aerosol. Another possibility would be that high NOx concentrations would prevent the formation of ozone, which would hinder SOA formation from aromatic species."

Reviewer comment

- There still seems to be a disconnect between the chemical analysis results and optical properties discussed here. Please see one of my comments below.
- L410(L420): When discussing the chemical analysis results, only that of acacia and eucalyptus are discussed. Wasn't analysis for the olive fuel carried out as well?

Author Response:

Analysis for the olive fuel was not carried out. Unfortunately, time and funding did not allow us to carry out this analysis. Additionally, a three-way comparison would be significantly more complex.

Reviewer comment

- L650 (L421): what's the basis of this statement: "Since it is Acacia that appears to have many more low-abundant organic constituents"? This goes back to my point that the composition data cannot be separated from this paper or else, the paper seems incomplete.
- Can authors include the uv-vis spectrum of the extract for different fuels and different burn conditions?

Author Response:

*The supporting information for this statement is now included in SI and is **Figure S5**. Identification for compounds with an absolute difference greater than 0.5% have been labeled and are listed in **Table S1**. References to this in the text have been made.*

Reviewer comment

- Can authors include the uv-vis spectrum of the extract for different fuels and different burn conditions?

Author Response:

*The authors have done this in **Figure S6**. References to this in the text have been made. Unlike in part 2, where the entire available wavelength range is discussed, the figures presented here focus on the 500-570 nm region of the spectrum.*

Reviewer specific comments:
- L719 (L461): change "at night" to "in the dark"

Author Response: *The change is made.*

Reviewer comment
-L-720 (L462) It will be valuable to show the change in aerosol size and density for the dark aging experiments in a plot.

Author Response:
*Unfortunately, we did not possess the APM at the time these experiments were made, so density measurements are not possible. For the size distributions, this is provided as heat maps for number density as a function of time for smoldering-dominated Acacia and Eucalyptus as they aged in the dark. This is **Figure S1** and has been referenced in the text.*

Reviewer comment

L745 (L497): nitrites or nitrates?

Author Response: *nitrates. This will be specified in the text.*

Reviewer comment
L720-745 (L464-470): since RH in the current experiments was low and not changing, the discussion about chemistry under higher RH seems irrelevant.

Author Response
The discussion about chemistry under higher RH was included since the focus of the work is on African biomass fuels, in a region where RH is high near the tropics. While our chamber RH was, low and was not representative of the tropics, we plan to conduct measurements at high RH as a follow up of this project.

Reviewer comment
- L793-794 (L498-499): This phrase is confusing: "(~12% by mass compared to ~12% from OH radical NO3 and ~76% from and proxy radical).

Author Response: *We have attempted to remedy this confusion.*

Changes made in the manuscript

"Only in the slow ignition case was there a significant formation of SOA from ozonolysis during dark aging (~12% by mass from ozonolysis compared to ~12% from OH radical NO_3 and ~76% from and proxy radical based on positive matrix factorization analysis)."

Reviewer comment

L920 (L543) I disagree; there are some chromophores that could be absorbing at longer wavelengths. Some of the chemical analysis discussion mentions presence of chromophores; if those analyses show only absorption at lower wavelengths, why include those results with the current study that focuses on extinction and scattering at 500-570 nm? How can the SSA of acacia and eucalyptus at these longer wavelengths be put in the context of the different types of chromophores that have been observed at lower wavelengths?

Author Response

In this paragraph, we are discussing the current state of knowledge in the field, and in this sentence, we were merely stating that this work does not cover the same wavelength range as previous studies. We would expect absorption features to extend to this region of the spectrum from shorter wavelengths, as demonstrated in the spectra we present.

Changes made in the manuscript

"These studies were made at wavelengths of 375 and 405 nm, while ours were done in the visible range, so they are not directly applicable to this work."

Reviewer comment

- L962 (L568): anthropogenic pollution is a very broad term. What was tested was only a mixture of 3 aromatic species. Please also see my comment above about NOx levels and SOA yields.

Author Response

The reviewer is correct: indeed, anthropogenic pollution is too broad to use in this work as we are using few examples of pollutants.

Changes made in the manuscript

The text will read

"The later would suggest that the three-aromatic species representing anthropogenic pollutants do not seem to affect the optical properties of BB aerosol."

Reviewer comment

- L 1008 (L601): What uncertainties about SMPS are they authors referring to? Can they be quantified?

Author Response

We were referring to the uncertainty in the counts measured by the CPC in the SMPS system. According to TSI, the uncertainty in the particle count by the WCPC is ±10%.

Changes made in the manuscript

The following sentence is added

"The uncertainty in the particle count by the WCPC is ±10%"

Reviewer #2

Suggestions for revision or reasons for rejection (will be published if the paper is accepted for final publication)

The study presents data on optical properties of biomass burning aerosols and on the effects dark- and photochemical aging on optical properties. The novelties of the study are the usage of sub-Saharan biomass fuels and the inclusion of the dark aging conditions in the experiments. The fact that dark aging affects optical properties in different way than photochemical aging is an important finding. Unfortunately, in the manuscript the experiments are quite poorly described both with respect to combustion conditions and chamber experiments. The combustion experiments are performed in a tube furnace using 0.5 g fuel pieces, which offers a good control over the combustion conditions. On the other hand, such a setup differs significantly from any real-world combustion appliance, both with respect to the combustion system geometry and the size of the fuel batch, which likely affects aerosol formation substantially. Therefore, a careful description the combustion conditions would be essential to make the results useful for the scientific community. Presently only MCE, which is a very simple metric depending on the exhaust CO concentration, is presented. The term "combustion temperature" is used throughout the manuscript without defining it (see detailed comments below). I would recommend to report at least the following data from the combustion experiments to make the data of this article more useful.

- Air-to-fuel ratio
- time-dependent CO, CO2 and hydrocarbon concentrations during combustion of the fuel batch
- Adiabatic combustion temperature

Moreover, the description of the experimental conditions in the chamber seem to be very limited. Clearly presented information on the concentrations of O3, non-methane VOC and NOx in the chamber (e.g. in a table) would be essential to understand the aging experiments. For UV-induced aging experiments, determination of the OH-radical exposure would be a benefit to relate the findings with other chamber experiments. It also seems that all experiments were not successful (e.g. concentrations were too low for some instruments to obtain data) and the authors conclude that further studies are needed.

The paper includes lot of discussion on the effects of particulate chemical composition on its optical properties. The discussed UPLC/DAD-ESI-HR-QTOFMS analyses of chemical constituents in the aerosols are very interesting and potentially very important for the scientific community. However, it is quite strange that no chemical data is presented in this paper and there are just citations to the "Part2-paper" where obviously, some of the discussed findings on chemical species are presented. In the current form, it is difficult for the reader to find the data since no figures or tables are referred to. In my opinion, if the chemical data is to be published in another paper, it would be more logical to publish first the chemical data. In any case, the discussed chemical data must be clearly visible for the readers. Overall, the paper addresses an important topic and presents potentially scientifically valuable results, but has some significant shortages in description of the experimental conditions and aerosol chemical compositions.

Author Response:

The authors are grateful for this reviewer's comments and pointing out the need for some clarification on engineering aspects of combustion theory and thermochemistry related to this work. We believe the comments and our responses improve the quality of the paper for publication in ACP. We address the comments one by one

- *The combustion apparatus is described in a later response.*

- *Hydrocarbon concentrations were not available during these experiments. However, in lieu of hydrocarbon measurements, we have made a plot for the temporal evolution of total particle mass in $\mu g/m^3$ assuming density of 1 gcm^{-3} , CO, and CO_2 concentration (both in ppmv) for smoldering-dominated Acacia and Eucalyptus. This is **Figure S2** and is referenced within the text. These measurements are following the smog chamber, so any high temporal resolution phenomenon would be lost upon mixing within the chamber.*

- *Regarding NOx and ozone, we were unable to measure those species during these experiments due to instrumentation issues. Based on the work of other researchers, (Akagi et al., 2012) we would expect no initial ozone production. The measurements mentioned in the manuscript were measurements done during the chamber characterization experiments.*

- *Regarding the lack of presented chemical data, we agree that this should not have been omitted and have taken great lengths to amend this shortcoming. A comparison of mass spectra for fresh emissions from Acacia and Eucalyptus are presented in **Figure S5** and **Table S2**. The effects of aging are demonstrated for smoldering-dominated Eucalyptus (**Figure S9a and Table S3**) and Acacia (**Figure S9b and Table S4**).*

Changes made in the manuscript

The following clarification is added in the manuscript

"The measurements of O_3 and NOx were done only during the chamber characterization experiments and were not measured in subsequent experiments reported in this work**"**

Reviewer comment

More specific comments are below:

Line 102: The authors state that they "have full control of temperature, airflow, and material combusted." If that is the case, more details on the combustion process should be available, than the single value of MCE, which has been provided in this paper. Moreover, the term "combustion temperature" is used throughout the manuscript without defining it (Pro tip: the tube furnace set point temperature is not necessarily the same as the combustion temperature). In general, during batch combustion of biomass there are many parameters affecting the composition of biomass burning PM, including, but not limited to:
- air-to-fuel ratio
- combustion rate
- fuel moisture content
- fuel particle size

- combustion chamber materials and geometry (these will influence the e.g. radiative heating of the fuel sample from the combustion chamber walls)
- residence time of the flue gases in the combustion appliance
- exhaust gas dilution temperature and dilution ratio
It would be important to include such information for example in the supplementary material

Authors Response

Our combustion apparatus has been thoroughly described in our previous characterization paper (Smith et al., 2019). Briefly, the furnace (Carbolite Gero, HST120300-120SN) holds an 85 mm OD, 80 mm ID, and 750 mm long quartz working tube and has a heated region of 300 mm. Stainless steel mounts and ceramic insulation plugs on either end enable the introduction and sampling of gasses. The furnace is preheated before the introduction of biomass samples. These samples are placed in a quartz combustion boat (AdValue Technology, FQ-BT-03), weighed and pushed into the center of the furnace with the aid of tongs, before replacing the input insulator and flange. The smoke and gasses produced from combustion are sent directly to the chamber via a heated (200 °C), and ¼-inch OD stainless steel bellows transfer tube. The combustion boat was 100 mm long, 41 mm wide, and 20 mm tall. ***The authors do not feel this level of detail is required in the current work, as the information is already readily available in a published form****.*

We calculated that the residence time of combustion gases within the tube furnace to be ~9.2 seconds. The dilution temperature and dilution ratio is not applicable, since a diluter was not used. Effluent from the tube furnace was sent directly to the smog chamber."

The authors agree that the term "combustion temperature" may be misleading. In this work, we mean the set point temperature of the furnace when the sample is first placed into the furnace. ***This will be reworded in Section 3.1 of the manuscript.*** *Further, we believe there is some confusion regarding the purpose of these experiments. We are using a furnace (described above) to ignite the fuel for generating biomass burning aerosol. We do not attempt to measure the properties or capability of the biomass as a fuel for use in cook stoves or combustion engines. While we agree with the reviewer that several of these quantities could be gathered from this data, we are unaware of any other research groups in atmospheric science using these values for biomass burning aerosol research. The paragraphs below are an attempt to provide this data for the reviewer, but we have chosen not to include this in the final manuscript since it is beyond the scope of our work.*

Although we do not have the exact elemental composition for the species used in this work, we can approximate them using data from Table 1 of Silva et al. (2019). For our purposes, the "branch" category most closely resembled what we burned in our lab. Acacia has a C:H:N:O:S ratio (by composition) of 0.483 : 0.0582 : 0.0228 : 0.4352 : 0.00067, while Eucalyptus has a respective ratio of 0.4412 : 0.0525 : 0.0133 : 0.4926 : 0.00035. This gives a stoichiometric air-to-fuel ratio of 3.18 for Acacia, and 2.28 for Eucalyptus. This assumes ideal conditions where the fuel is completely combusted. The actual air to fuel ratio also requires complete measurement of hydrocarbons, total particle mass, and elemental particle composition which we did nott have.

Changes made in the Supplementary Document

The following information will be provided in the supplementary document.

The combustion time for our fuels was between 5 and 10 minutes. The exact time is unknown since we could not see into the furnace during combustion. The ash left on boat was less than 3% of the fuel mass.

Heat transfer to wood particles is directly proportional to the exposed surface area of the sample. Smaller particles have a larger surface area to mass ratio than larger particles. This in turn means a faster rate of heat transfer to the particles and, consequently, a faster combustion rate. (Simmons, 1983). In this work, small twigs were used for combustion, fuel particle size can be approximated as a cylinder of mass 0.5 g, with an average radius of 0.25 cm and an average length of less than 5 cm, giving an upper limit of 0.0012 m^3 for the volume, an upper limit of 0.000825 m^2 for the exposed surface area of the fuel, and a lower limit of 0.405 kg/m^3 for the density of the fuel used. Typically, whole twigs with a thin layer of bark were used, although occasionally two or more smaller pieces may have been used to achieve the same mass. Occasionally, these twigs were also split open. These factors could increase the surface area of the fuel by approximately 0.000325 m^2 for the same fuel mass.

We calculate that the residence time of combustion gases within the tube furnace is ~9.2 seconds. The dilution temperature and dilution ratio is not applicable, since a diluter was not used. Effluent from the tube furnace was sent directly to the smog chamber.

Changes made in the manuscript:

We will clarify the definition of "combustion temperature" on Lines 341-343. It should now read: "Each fuel was placed into the tube furnace set at two different temperatures (initially heated at 500 ℃ and 800 ℃) to investigate the impact of ignition temperature on aerosol optical properties and chemical composition. In both cases, the furnace was allowed to reach the desired temperature before the sample was placed inside."

"The moisture content of the biomass fuel samples was 10%."

Reviewer comment

Line 119: "0.5 g of fuel was burned normally, which produced about 600 to 800 μg m-3 of mass loading in the chamber". As the chamber volume is 9 m3, the particulate mass derived from the 0.5 g batch is up to 7200 ug, which equals to particulate emission factor of 14400 mg/kg fuel. This is a quite high emission factor for any combustion system. The authors should discuss the relevance of this result in the paper.

Authors Response

We thank the reviewer for the comments. We don't think 14400 mg/kg (14.4 g/kg) of emission factor is quite high for smoldering fires. For example, Liu et al. (2017) reported average EFs of PM1 as 26 ± 6.2 g/kg in western US wildfires. In addition, Akagi et al. (2011) reported PM EFs for Boreal, Temperate, and Extratropical forests as larger than 15 g/kg. So, we are confident that the ranges of EFs we are getting for smoldering dominated burns are within the ranges estimated by past studies as reported in the current literature.

Reviewer comment

Line 135: “For this work, only zero air was used at a flow rate of 10 sL min–1.”
What was the air-to-fuel ratio? Why air was used, although there was a possibility to use lower oxygen contents?

Authors Response:

As mentioned in a previous response, the air-to-fuel ratio was between 2.28 and 3.18 for the fuels used in this study. Reducing the oxygen content is certainly within our experimental capacity. However, it has not yet been explored as a variable. We found that temperature alone was enough to distinguish between smoldering and flaming combustion for our experiments.

Reviewer comment

Line 139: “the tube furnace provides a uniform temperature throughout the sample.”
What is the basis for this argumentation? How much is the heat released by the burning fuel particle in comparison to the heat fluxes from the tube furnace walls? The adiabatic combustion temperatures could be calculated based on the fuel composition, air-to-fuel ratios and external heat from the tube furnace walls.

Authors Response:

This statement was based on the tube furnace specification, as there is a temperature gradient in the tube that provides a uniform heated region of 300 mm, in which the sample boat resides. The concept of Adiabatic combustion or flame temperature is generally used as an engineering design criterion for air –firing combustion chambers and power plants. This quantity is not generally reported in aerosol research and we fail to see the relevance to the work reported here.

This quality is generally easy to calculate for gaseous fuels. Information on the composition of liquid or solid fuels is generally much more limited than that for gaseous fuels. Physical and chemical properties of a wood, such as chemical composition and thermal properties, play an important role in its combustion. However, based on available information we have calculated the adiabatic flame (combustion) temperature and was 3706 °C and 3679 °C for acacia and eucalyptus, respectively.

.

The following is included in the supplementary information:
The adiabatic flame (combustion) temperature is 3706 °C and 3679 °C for acacia and eucalyptus, respectively.
Changes made in the manuscript: *The following sentence is added to clarify the temperature uniformity.*
*“*as the tube provides a uniform heated region of 300 mm which is approximately the size of the quartz boat.”

Reviewer comment

Line 193: “Aerosol growth in the chamber was expected to be due to coagulation, diffusional losses of particles,” This is already mentioned on the line 184. -> the factors related to particle

growth are unnecessary repeated.

Author's Response. *The reviewer is correct. The text is edited to remove repetition*.

Reviewer comment
Line 206: Please considering putting the section "2.1.3 Chamber cleaning" into the supporting material, as it consists only of technical details on the implementation of the experiments.

Author's Response:
We agree with the reviewer. Chamber cleaning and other additional experimental details are included in the supplemental section.

Reviewer comment

Line 222: "Optical properties were measured using the procedure described below soon after the chamber was well mixed." This is not a very informative sentence.

Authors Response: *We agree with the reviewer.*

Changes made in the manuscript: *The text will be rewritten to read:*
"Optical properties for fresh samples were measured using the procedure described below within 90 minutes of combustion, which allowed the size distribution of the aerosol to stabilize enough to conduct measurements without having a significant change in number density over the course of the experiment."

Reviewer comment

Line 224: "For the photochemical aging, a new burn was made, and the particles were kept in the chamber for 12 hours with the UV lights on." What does it mean that a new burn was made? How is this experiment different from the dark aging, apart from the fact that the UV-lights were on, remains unclear.

Authors Response
For the dark aged experiments, the sample was left in the chamber after fresh measurements were made. For photochemically aged experiments, a new sample was needed, since the original sample had already been altered by dark aging. Due to the length of time necessary to make fresh measurements, these were not conducted for the photochemically aged sample; instead, the UV lights were turned on immediately after combustion, and the sample was allowed to age for 12 hours before taking any measurements. The reviewer is correct that the only difference in the aging experiments is the presence of UV radiation, which is the only variable that changes. The manuscript will be edited for clarity.

Changes made in the manuscript: *The text will be rewritten to read:*
"For photochemical aging, a fresh sample was introduced into a clean chamber with the UV lights on immediately after combustion. Measurements were made after 12 hours of UV radiation*."*

Reviewer comment

Line 229-: I suggest to start the paragraph by explaining how the experiment "in a polluted environment" is different to an experiment "clean environment". In the present form the reader patiently has to go through lot of technical details related to measurement accuracy etc. before even knowing how these experiments were performed. It also remains unclear whether the VOC:s were injected into the chamber before or after feeding the BB-smoke sample? How did adding of VOC:s affect the NMVOC:NOx -ratio in the chamber? Are the NMVOC:NOx -ratios representative to the air of the South African sites in question?

Authors Response:

We agree with the reviewer about the introduction to this section. As mentioned in the response to a previous comment, hydrocarbon concentrations were unavailable for these experiments.

Changes made in the manuscript: *The following paragraph will be added at Line 229:*
"To study the effect of photochemical aging in a polluted environment, a mixture of VOCs was used to simulate an urban atmosphere. These VOCs were injected into the chamber and allowed to mix with the chamber air while the furnace heated up before the introduction of fuel samples. The rest of this section describes the preparation of this VOC mixture."

Reviewer comment

Line 397-399: It is not possible to define the chemical composition of particles, based on the MCE. MCE is a very simple metric depending on the exhaust CO concentration. Generally, there is no good correlation between CO and OC/BC in biomass combustion. In my opinion the authors should present measured data on BC and OC concentrations to state such findings. The color of the filter is not a very scientific method for chemical characterization of aerosol particles.

Authors Response

We agree with the reviewer that correlation of CO is not very good with OC/BC. But for biomass burning emissions, for lower MCE (< 0.9), the fraction of BC is very low (below 10% or so), whereas for higher MCE (>0.98), the fraction of BC is significantly higher. So, we still think we can say that less BC is produced during smoldering combustion, whereas more BC is produced during flaming combustion as in previous studies (Lewis et al., 2008;Liu et al., 2014;Pokhrel et al., 2016;McMeeking et al., 2014;Stockwell et al., 2016) We agree with the reviewer that color of the filter is not a scientific method for chemical characterizations but we can clearly say that if the color of the filter is black then the emission is dominated by the BC; otherwise it will not look black. The intent for showing the filters was illustrative, not quantitative.

Changes made in the manuscript: *The text will be rewritten to read:*

"A qualitative visual measure of the impacts of combustion temperature on aerosol properties can also be gleaned by looking at the color of the collected filter samples, as shown in Figure S4."

Reviewer comment

Line 430-433: "Chemical analysis revealed that for smoldering-dominated combustion, Eucalyptus and Acacia had a variety of compounds in common, such as lignin pyrolysis products, distillation products, and cellulose breakdown products. Several lignin pyrolysis products and distillation products are more prevalent in Eucalyptus than in Acacia, while pyrolysis products of cellulose and at least one nitroaromatic species were more prevalent in Acacia." Please refer to a table or figure where this information can be seen in a numerical form.

Authors Response:

This information is now provided in supplementary information. Figures (difference mass spectra) are provided in Figures S5 and S9. The accompanying tables (S2, S3, and S4) give the quantitative information for each peak, and suggested identities. Additionally, for each suggested identity, there is a compound type listed (lipid, lignin pyrolysis product, distillation products, sugar/cellulose product, nitro-aromatic compound, oxidized polyaromatic hydrocarbon, and oxidized anthropogenic volatile organic compound).

Reviewer comment

Line 467: "BB aerosol was aged without UV lights on and kept overnight for 24 hours."
This is not much information about the conditions during the experiment. What was the ozone concentration during the dark aging period? Was O3 added into the chamber? Later (Line 481) it is argued that oxidation of organic aerosol was initiated by O3. Is there no measured information on O3 ? That would be a notable shortage to describe the experimental conditions.

Authors Response

We thank the reviewer for constructive comments. As expected, ozone is a secondary product formed in biomass burning smoke(Akagi et al., 2012) and there was no ozone initially. Furthermore, during dark aging, production of ozone is not expected in the absence of radiation.

Changes made in the manuscript; *Line 467 now read as "*BB aerosol was aged in dark for 24 hours in absence of UV lights and additional ozone*". We edited Line 481 which now reads as* "The potential mechanism for the observed result could be due to the formation of less/non-absorbing secondary organic aerosol".

Reviewer comment

Line 570-573: Data on the concentrations of chemical species in the chamber should be presented in this paper to discuss the findings.

Author's Response:

Regarding the chemical constituents discussed in this section (i.e. those in the particulate phase), this information has been provided, as indicated earlier. References to SI have been included in the text.

Reviewer comment
Line 598-599: "Our connecting tubing was short enough (0.5 m) to neglect such a loss." What is the basis for this conclusion? The length of the tube cannot be used as a proof of low losses.

Author's Response:
The tubing that transports the smoke between the burn chamber and the smog chambers is also susceptible to losses/ delays of gas-phase SOA-precursor material (Pagonis et al., 2017). Losses of ultrafine (those below 100 nm) particles inside the sampling tubes were observed, with smaller particles suffering greater losses (Kumar et al., 2008) Furthermore, they showed relatively greater losses of particles with increased length of sampling tubes. The basis of the conclusion is the citations mentioned Kumar et. al will be included in the revision.

.

Completion Date: 6/30
*there may need to be a separate section on "changes to the manuscript" after the author response

References:

Akagi, S. K., Yokelson, R. J., Wiedinmyer, C., Alvarado, M. J., Reid, J. S., Karl, T., Crounse, J. D., and Wennberg, P. O.: Emission factors for open and domestic biomass burning for use in atmospheric models, Atmos. Chem. Phys., 11, 4039-4072, 10.5194/acp-11-4039-2011, 2011.

Akagi, S. K., Craven, J. S., Taylor, J. W., McMeeking, G. R., Yokelson, R. J., Burling, I. R., Urbanski, S. P., Wold, C. E., Seinfeld, J. H., and Coe, H.: Evolution of Trace Gases and Particles Emitted by a Chaparral Fire in California, Atmos. Chem. Phys., 12, 1397, 2012.

Kumar, P., Fennell, P., Symonds, J., and Britter, R.: Treatment of losses of ultrafine aerosol particles in long sampling tubes during ambient measurements, Atmospheric Environment, 42, 8819-8826, https://doi.org/10.1016/j.atmosenv.2008.09.003, 2008.

Lewis, K., Arnott, W. P., Moosmüller, H., and Wold, C. E.: Strong spectral variation of biomass smoke light absorption and single scattering albedo observed with a novel dual-wavelength photoacoustic instrument, Journal of Geophysical Research: Atmospheres, 113, 10.1029/2007jd009699, 2008.

Liu, S., Aiken, A. C., Arata, C., Dubey, M. K., Stockwell, C. E., Yokelson, R. J., Stone, E. A., Jayarathne, T., Robinson, A. L., DeMott, P. J., and Kreidenweis, S. M.: Aerosol single scattering albedo dependence on biomass combustion efficiency: Laboratory and field studies, Geophysical Research Letters, 41, 742-748, 10.1002/2013GL058392, 2014.

Liu, X., Huey, L. G., Yokelson, R. J., Selimovic, V., Simpson, I. J., Müller, M., Jimenez, J. L., Campuzano-Jost, P., Beyersdorf, A. J., and Blake, D. R.: Airborne Measurements of Western US

Wildfire Emissions: Comparison with Prescribed Burning and Air Quality Implications, J. Geophys. Res. D: Atmos., 122, 6108, 2017.

McMeeking, G. R., Fortner, E., Onasch, T. B., Taylor, J. W., Flynn, M., Coe, H., and Kreidenweis, S. M.: Impacts of nonrefractory material on light absorption by aerosols emitted from biomass burning, Journal of Geophysical Research: Atmospheres, 119, 12,272-212,286, 10.1002/2014jd021750, 2014.

Pagonis, D., Krechmer, J. E., de Gouw, J., Jimenez, J. L., and Ziemann, P. J.: Effects of gas–wall partitioning in Teflon tubing and instrumentation on time-resolved measurements of gas-phase organic compounds, Atmos. Meas. Tech., 10, 4687-4696, 10.5194/amt-10-4687-2017, 2017.

Pankow, J. F.: Review and comparative analysis of the theories on partitioning between the gas and aerosol particulate phases in the atmosphere, Atmospheric Environment (1967), 21, 2275-2283, https://doi.org/10.1016/0004-6981(87)90363-5, 1987.

Pokhrel, R. P., Wagner, N. L., Langridge, J. M., Lack, D. A., Jayarathne, T., Stone, E. A., Stockwell, C. E., Yokelson, R. J., and Murphy, S. M.: Parameterization of single-scattering albedo (SSA) and absorption Ångström exponent (AAE) with EC / OC for aerosol emissions from biomass burning, Atmos. Chem. Phys., 16, 9549-9561, 10.5194/acp-16-9549-2016, 2016.

Radney, J. G., and Zangmeister, C. D.: Practical limitations of aerosol separation by a tandem differential mobility analyzer–aerosol particle mass analyzer, Aerosol Science and Technology, 50, 160-172, 10.1080/02786826.2015.1136733, 2016.

Ranjan, M., Presto, A. A., May, A. A., and Robinson, A. L.: Temperature Dependence of Gas–Particle Partitioning of Primary Organic Aerosol Emissions from a Small Diesel Engine, Aerosol Science and Technology, 46, 13-21, 10.1080/02786826.2011.602761, 2012.

Silva, D. A. d., Eloy, E., Caron, B. O., and Trugilho, P. F.: Elemental Chemical Composition of Forest Biomass at Different Ages for Energy Purposes, Floresta e Ambiente, 26, 2019.

Simmons, W. W.: Analysis of Single Particle Wood Combustion in Convective Flow, PhD, University of Wisconsin, Madison, WI, 1983.

Smith, D. M., Fiddler, M. N., Sexton, K. G., and Bililign, S.: Construction and Characterization of an Indoor Smog Chamber for Measuring the Optical and Physicochemical Properties of Aging Biomass Burning Aerosols, Aerosol and Air Quality Research, 19, 467-483, 10.4209/aaqr.2018.06.0243, 2019.

Stockwell, C. E., Christian, T. J., Goetz, J. D., Jayarathne, T., Bhave, P. V., Praveen, P. S., Adhikari, S., Maharjan, R., DeCarlo, P. F., Stone, E. A., Saikawa, E., Blake, D. R., Simpson, I. J., Yokelson, R. J., and Panday, A. K.: Nepal Ambient Monitoring and Source Testing Experiment (NAMaSTE): emissions of trace gases and light-absorbing carbon from wood and dung cooking fires, garbage and crop residue burning, brick kilns, and other sources, Atmos. Chem. Phys., 16, 11043-11081, 10.5194/acp-16-11043-2016, 2016.

Wei, W., Mandin, C., Blanchard, O., Mercier, F., Pelletier, M., Le Bot, B., Glorennec, P., and Ramalho, O.: Temperature dependence of the particle/gas partition coefficient: An application to predict indoor gas-phase concentrations of semi-volatile organic compounds, Science of The Total Environment, 563-564, 506-512, https://doi.org/10.1016/j.scitotenv.2016.04.106, 2016.

Weschler, C. J., and Nazaroff, W. W.: Semivolatile organic compounds in indoor environments, Atmospheric Environment, 42, 9018-9040, https://doi.org/10.1016/j.atmosenv.2008.09.052, 2008.

Laboratory studies of fresh and aged biomass burning aerosols emitted from east African biomass fuels-PART 1-Optical properties

Damon M. Smith,[1,2,#] Marc N. Fiddler[3], Rudra P. Pokhrel[1], Solomon Bililign[1*]

1. Department of Physics, North Carolina Agricultural and Technical State University, Greensboro, NC, 27411 USA,
2. Applied Sciences and Technology Program, North Carolina A&T State University, Greensboro, NC 27411, USA,
3. Department of Chemistry, North Carolina Agricultural and Technical State University, Greensboro, NC, 27411, USA

Current address: Department of Chemistry and Physics, Western Carolina University, Cullowhee, NC 28723
* Correspondence: Bililignsol@gmail.com; Tel.: (+13362852328);

Abstract: An accurate measurement of the optical properties of aerosol is critical for quantifying the effect of aerosol on climate. Uncertainties persist and measurement results vary significantly. Biomass burning (BB) aerosol have been extensively studied through both field and laboratory environments for North American fuels to understand the changes in optical and chemical properties as a function of aging. There is a clear research need for a wider sampling of fuels from different regions of the world for laboratory studies. This work represents the first such study of the optical and chemical properties of wood fuel samples used commonly for domestic use in east Africa. In general, combustion temperature or modified combustion efficiency (MCE) plays a major role on the optical properties of the emitted aerosols. For fuels combusted with MCE of 0.974 ± 0.015 referred to as flaming-dominated combustion, the single scattering albedo (SSA) values were in the range between 0.287 to 0.439, while for fuels combusted with MCE of 0.878 ± 0.008 referred to as smoldering-dominated combustion the SSA values were in the range between 0.66 to 0.769. There is a clear but very small dependence of SSA on fuel type. A significant increase in the scattering and extinction cross-section (with no significant change in absorption cross-section) was observed, indicating the occurrence of chemistry, even during dark aging for smoldering-dominated combustion. This fact cannot be explained by the heterogeneous oxidation in particle phase and we hypothesize that secondary organic aerosol formation is potentially happening during dark aging. After 12 h of photochemical aging, BB aerosol become highly scattering with SSA values above 0.9, which can be attributed to oxidation in the chamber. Aging studies of aerosol from flaming-dominated combustion, were inconclusive due to the very low aerosol number concentration. We also attempted to simulate polluted urban environments by injecting volatile organic compounds (VOCs) and BB aerosol into the chamber, but no distinct difference was observed when compared to photochemical aging in the absence of VOCs.

Deleted: s

Deleted: s

Deleted: s

Deleted:

Deleted:

1 Introduction

The role of biomass burning (BB) aerosols on air quality, human health, cloud formation, and climate remain poorly quantified. BB aerosol play an important role in the earth's radiation budget and in the hydrological cycle by

absorbing and scattering sunlight and by providing nuclei for cloud condensation (Crutzen and Andreae, 1991). There have been several estimates of the radiative forcing of BB aerosols ranging from 0.03 ± 0.12 W m^2 (Forster et al., 2007) to the most recent estimate of −0.2 W m^{-2} (Boucher, 2013). The uncertainty associated with the radiative forcing, is in the range of –0.07 to –0.6 W m^{-2} (IPCC, 2014). This high level of uncertainty is associated with uncertainty in measuring the optical properties of BB aerosol (Andreae and Merlet, 2001;Koch et al., 2009;IPCC, 2014). In most cases, the measurements of aerosol optical properties are either limited to a specific source region or confined to a limited wavelength range. Internally versus externally mixed particles can have very different optical properties (e.g.,(Jacobson, 2000;Stier et al., 2006;Schwarz et al., 2008)). The processing of fire emissions leading to the eventual formation of secondary organic aerosols (SOA) is complex, including dilution, partial evaporation of the primary organic aerosols (POA) into gaseous species, photochemical reactions of organic species, partitioning of semi-volatile primary emissions into the condensed phase upon cooling, and multiphase chemical conversion (including cloud processing) (Bruns et al., 2016).

Furthermore, it is often wrongly assumed that the only two aerosols that contribute significantly to light absorption on a global scale are black carbon (BC) and mineral dust. Current climate models fail to recognize that organic aerosols (OA) is not purely scattering (Bond et al., 2011;Ma et al., 2012;Bahadur et al., 2012;Laskin et al., 2015). Rather, there is a growing amount of data indicating that a certain class of OA, known as brown carbon (BrC), can be commonly found on a global scale, particularly in urban environments, where it contributes significantly to the total aerosol absorption- specifically in the lower visible and ultraviolet wavelength range, where BC absorbs weakly (Chung et al., 2012;Kirchstetter et al., 2004;Yang et al., 2009;Laskin et al., 2015). Global simulations suggest that this strongly absorbing BrC contributes from +0.12 to +0.25 W m^{-2} or up to 19% of the absorption by anthropogenic aerosols (Feng et al., 2013;Brown et al., 2018;Saleh et al., 2015;Saleh et al., 2014).

The environmental and health costs of pollutants emitted from open biomass burning and cookstoves are significant and have been associated with human health effects, including early deaths and low infant birth weight. There is a strong evidence for acute respiratory illnesses such as asthma, and chronic obstructive pulmonary disease (COPD) associated with open biomass burning (Naeher et al., 2007;Stefanidou et al., 2008;Holstius et al., 2012;Johnston et al., 2012;Johnston et al., 2011;Elliott et al., 2013;Henderson et al., 2011;Delfino et al., 2009;Rappold et al., 2011;Sutherland et al., 2005;Smith and Pillarisetti, 2017). Wildfire can have health impacts well beyond the perimeter of the fire even thousands of miles downwind (Spracklen et al., 2009).

This work is focused on biomass fuels from east Africa. It is estimated that nine out of ten, or 573 million people in sub-Saharan Africa, will remain without access to electricity by 2030 (Bank, 2019). The African continent is the largest source of BB emissions, with recent studies estimating African contributions to be ~55% of total global emissions of BB aerosols (Ichoku et al., 2008;Roberts et al., 2009;Roberts and Wooster, 2008;Lamarque et al., 2010;van der Werf et al., 2010;Schultz et al., 2008). African combustion emissions are expected to grow. For example, organic carbon (OC) emissions from Africa, are expected to make up 50% of the total global emissions in 2030 (Liousse et al., 2014). Africa currently has the fastest growing population in the world; projected to more than double between 2010 and 2050 (UN, 2011).

Deleted:

Deleted:

Deleted:

Deleted:

BB is a global phenomenon, and it was shown that the long-range transport of pollutants emitted from BB can affect air quality very far from the source (Edwards et al., 2006;Williams et al., 2012). Although the optical properties of BB aerosols emitted by biomass species native to North America have been extensively investigated (Hodzic et al., 2007;Yokelson et al., 2009;Liu et al., 2014;McMeeking et al., 2009;Levin et al., 2010;Mack, 2008;Mack et al., 2010), biomass fuels native to sub-Saharan Africa have only been studied during a few field campaigns (Eck et al., 2001;Liousse et al., 2010;Formenti et al., 2003). Due to the very limited available data, the models being used for air quality and climate change in Africa rely on global inventories, which are primarily collected from North America, Europe and Asia (Bond et al., 2004;Streets et al., 2004;Bond et al., 2007;Klimont et al., 2009;Lamarque et al., 2010;Klimont et al., 2013), and are not consistent with satellite observations over Africa (Liousse et al., 2010;Malavelle et al., 2011;Liousse et al., 2014).

To our knowledge, laboratory studies of the optical properties of BB aerosols from solid wood biomass fuels common for domestic use in east Africa have not been conducted. The only other African fuel studied were savannah grass from South Africa during FLAME-4 (Pokhrel et al., 2016) and savannah grass from Namibia and Brachystegia spiciformis from Zimbabwe during the Impact of Vegetation Fires on the Composition and Circulation of the Atmosphere (EFEU) project (Hungershoefer et al., 2008). With the exception of these two examples almost all reported laboratory studies have been focused predominantly on North American fuels (Hodshire et al., 2019). To improve air quality and climate change models for Africa, there is a need for laboratory studies to measure optical properties of BB aerosols from African fuel sources as the aerosols age and interact with polluted air that has the same chemical profile as African megacities and rural areas.

Smog chambers provide a controlled environment for a comprehensive study of aerosol optical properties, chemical and morphological evolution, and SOA formation. While fuel specific studies cannot be easily compared to wildfire field studies (Akagi et al., 2012), they can be used to compare emissions from domestic biomass use where the fuel type is known and is often not mixed. It is suggested that burn conditions influence emissions and aerosol mass (Yokelson et al., 2013;Liu et al., 2017) and may be a key difference between laboratory and field studies. To extend the results from this kind of study to more realistic conditions, we compare our results to previous parameterization schemes. In our work, we use a tube furnace for initiating the burn, where we have full control of temperature, airflow, and material combusted. Comparative laboratory studies of BB aerosol optical properties using fuels from Africa and higher latitudes under varying conditions and background pollutant abundances and photochemical aging will provide information on factors most critical for radiative impacts of BB aerosols.

In the first part of his study, we report the results from three biomass fuels from east Africa considered for a systematic fuel-specific study of optical properties of BB aerosols under different aging and burning conditions using an indoor smog chamber. Optical properties were measured for BB aerosols produced under smoldering-dominated and flaming-dominated combustions for each fuel type. For each combustion condition, we report the measured optical properties (i.e. scattering and extinction cross-sections, and single scattering albedo (SSA)) for fresh emissions, dark aged, photochemically aged and photochemically aged, with added VOC's to represent urban emissions from a representative African megacity.

2 Experimental methods

For this study, authentic hard wood fuels were obtained from east Africa and left under a hood to dry out for over a year. The fuel moisture content of less than 10%. These samples were weighed on a calibrated analytical balance so that it would approximately yield a total aerosol loading representative of a scenario (urban, wildfire, etc.).

2.1 BB aerosol generation

For laboratory samples, BB aerosol were generated by combusting wood samples in a tube furnace. This process has been described elsewhere in detail and is summarized here for clarity (Poudel et al., 2017;Smith et al., 2019). Samples with a mass of 0.5 g were typically used for experiments, which generally produces enough BB aerosol for optical property measurements without overloading any of the instruments. The mass loading was estimated by determining the total aerosol volume, obtained by measuring the volume distribution with a scanning mobility particle sizer (SMPS) and assuming a density of 1 g cm^{-3} for fresh aerosol. Samples as small as 0.1 g and as large as 5 g have been used before, with the maximum mass loading for the tube furnace near 10 g. Biomass samples were placed in a quartz combustion boat (AdValue Technology, FQ-BT-03), which was in turn placed at the center of the working tube inside the furnace (Carbolite Gero, HST120300-120SN). The tube furnace was set at 500 ^{o}C and 800 ^{o}C for each fuel. Unlike the heating coils used to initiate burning (Sumlin et al., 2018) where the temperature is uneven and localized, the tube furnace provides a uniform temperature throughout the sample as the tube provides a uniform heated region of 300 mm which is approximately the size of the quartz boat. Oxygen content can be varied between ambient conditions and the oxygen-starved conditions found within forest fires by mixing air from a zero-air generator (Aadco Instruments, 747-30) with nitrogen. Flows from both gases are regulated by calibrated mass flow controllers (MFC, Sierra Instruments). For this work, only zero air was used at a flow rate of 10 sL min^{-1}. Details of combustion characteristics including, fuel moisture content, fuel particle size, residence time and adiabatic combustion temperature are provided in the supplementary document (ST-2).

MCE were calculated from CO and CO_2 measurements. These measurements underwent external calibration with either a pure gas (for CO_2) or a certified standard (199.7 ppm for CO and 5028 ppm for CO_2, purchased from Airgas National Welders). Gas filter correlation analyzers from Thermo Scientific were used to measure CO and CO_2 (models 48C and 41C, respectively). The change in the CO and CO_2 concentration was determined by comparing average measurements before a burn, and after the burn, once the measurements were stabilized. Averages of increase in concentration were taken soon after the measurements were stabilized, but before dilution could take place. Between 80s and 300s measurements at 10 Hz were averaged for the pre-burn state, and ~300s for the post-burn state. MCE was determined by the following equation:

$$MCE = \frac{\Delta[CO_2]}{\Delta[CO_2]+\Delta[CO]} \quad (1)$$

The average modified combustion efficiency (MCE) for the 500 °C burn was 0.878 ± 0.008, which is hereafter referred to as smoldering-dominated combustion. For 800 °C burn case the average MCE was 0.974 ± 0.015,

Formatted: Indent: First line: 0.5"
Deleted: ,
Deleted: expected to retain little to no moisture content
Deleted: During all the experiments, 0.5 g of fuel was burned normally, which
Moved down [1]: produced about 600 to 800 µg m^{-3} of mass loading in the chamber. The mass loading was estimated by determining the total aerosol volume, obtained by measuring the volume distribution with a scanning mobility particle sizer (SMPS) and assuming a density of ... [1]
Deleted:
Formatted: Don't adjust space between Latin and Asian text, Don't adjust space between Asian text and numbers
Moved (insertion) [1]
Deleted: produced about 600 to 800 µg m^{-3} of mass loading in the chamber.
Deleted:
Deleted:
Formatted: Superscript
Formatted: Superscript
Formatted: Pattern: Clear
Formatted: Left, Indent: First line: 0"
Formatted: Don't adjust space between Latin and Asian text, Don't adjust space between Asian text and numbers

which is hereafter referred to as flaming-dominated combustion. The 0.5 g fuel produced about 600 to 800 μg m^{-3} of mass loading in the chamber during smoldering-dominated combustion.

2.2. Indoor smog chamber and characteristics

The North Carolina Agricultural and Technical State University (NCAT) indoor smog chamber has a volume of 9.01 m^3 and is lined by Fluorinated ethylene propylene (FEP) Teflon. Two sides each have a bank of 32 ultraviolet (UV) lights (Sylvania, F30T8/350BL/ECO, 36"), for a total of 64 lamps. Emissions from combustion (gas and particles) were transferred to the smog chamber via heated (200° C), ¼ inch stainless steel tubing, after which they undergo cooling and dilution in a natural fashion rather than a stepwise process. A mixing fan was used to produces a well-mixed volume within 10 to 20 minutes after combustion. In these experiments, the fan ran for 10 minutes while smoke was being introduced to the chamber, then for another 10 minutes after the furnace had been disconnected from the chamber. The chamber was constantly diluted by zero air (from generator). The flow rate was varied depending on the sampling demands of instrumentation but was usually around 4 L min^{-1} for a normal cavity ring down spectroscopy (CRDS) experiment.

The smog chamber was constructed to sample several particulate and gas-phase species. Ozone (O_3) was measured with a Thermo-Environmental Instruments UV photometer (model 49), and NO_x was measured with a Monitor Labs fluorescence analyzer (model 8840). The O_3 and NO_x analyzer signals were digitized with a DAQ (National Instruments, USB-6002) and the signal was displayed and stored via custom software (LabVIEW). The measurements of O_3 and NO_x were done only during the chamber characterization experiments and were not measured in subsequent experiments reported in this work.

Several parameters concerning our chamber itself have already been determined and reported (Smith et al., 2019). Chamber performance is affected by the intensity and spectral character of radiation, surface-to-volume ratio, and nature and condition of the wall surface (Hennigan et al., 2011). For our chamber, wall-loss rates of NO, NO_2, O_3 and PM were determined. Total light intensity was determined in a separate experiment by measuring photolysis of NO_2 and knowing the spectral output of the UV lamps. The wall loss rates for NO, NO_2, and O_3 were found to be $(7.40 \pm 0.01) \times 10^{-4}$, $(3.47 \pm 0.01) \times 10^{-4}$, and $(5.90 \pm 0.08) \times 10^{-4}$ min^{-1}, respectively. The NO_2 photolysis rate constant was 0.165 ± 0.005 min^{-1}, which corresponds to a flux of $(7.72 \pm 0.25) \times 10^{17}$ photons nm cm^{-2} s^{-1} for 296.0 – 516.8 nm, and the particle deposition rate was $(9.46 \pm 0.18) \times 10^{-3}$ min^{-1} for 100 nm mobility diameter BB particles from pine (Smith et al., 2019). Total aerosol surface area peaks approximately 20 minutes after combustion, while total aerosol volume peaks approximately 45 minutes after combustion. The aerosol appears to be well mixed within 20 minutes of combustion, with the size distribution resolving into a single lognormal distribution. However, this distribution continues to shift towards larger particle sizes, even after remaining in the smog chamber for over 24 h, as shown in Figure S3 for the smoldering-dominated combustion of Acacia and Eucalyptus. The gas and particle loss rates and other properties for our chamber are comparable to similar indoor smog chambers previously reported e.g. (Babar et al., 2016;Leskinen et al., 2015;Wang et al., 2014;Paulsen et al., 2005)). The temporal evolution of total particle mass, CO, and CO_2 concentration is shown in Figure S2 for smoldering-dominated Acacia and Eucalyptus. Chamber pressure and temperature did not vary much from room pressure and temperature during these experiments.

Deleted: Unlike the heating coils used to initiate burning (Sumlin et al., 2018) where the temperature is uneven and localized, the tube furnace provides a uniform temperature throughout the sample.

Deleted: MCE were calculated from CO and CO_2 measurements. These measurements underwent external calibration with either a pure gas (for CO_2) or a certified standard (199.7 ppm for CO and 5028 ppm for CO_2, purchased from Airgas National Welders). Gas filter correlation analyzers from Thermo Scientific were used to measure CO and CO_2 (models 48C and 41C, respectively). The change in the CO and CO_2 concentration was determined by comparing average measurements before a burn, and after the burn, once the measurements were stabilized. Averages of increase in concentration were taken soon after the measurements were stabilized, but before dilution could take place. Between 80s and 300s measurements at 10 Hz were averaged for the pre-burn state, and ~300s for the post-burn state. MCE was determined by the following equation:

Formatted: Justified

Moved down [2]: The North Carolina Agricultural and Technical State University (NCAT) indoor smog chamber has a volume of 9.01 m^3 and is lined by Fluorinated ethylene propylene (FEP) Teflon. Two sides each have a bank of 32 ultraviolet (UV) lights (Sylvania, F30T8/350BL/ECO, 36"), for a total of 64 lamps. Emissions from combustion (gas and particles) were transferred to the smog chamber via heated (200° C), ¼ inch stainless steel tubing, after which they undergo cooling and dilution in a natural fashion rather than a stepwise process. A mixing fan was used to produces a well-mixed volume within 10 to 20 minutes after combustion. In these experiments, the fan ran for 10 minutes while smoke was being introduced to the chamber, then for another 10 minutes after the furnace had been disconnected from the chamber. The chamber was constantly diluted by zero air (from generator). The flow rate was varied depending on the sampling demands of instrumentation but was usually around 4 L min^{-1} for a normal cavity ring down spectroscopy (CRDS) experiment.

Deleted: MCE were calculated from CO and CO_2 measurements. These measurements underwent external calibration with either a pure gas (for CO_2) or a certified standard (199.7 ppm for CO and 5028 ppm for CO_2, purchased from Airgas National Welders). Gas filter correlation analyzers from Thermo Scientific were used to measure CO and CO_2 (models 48C and 41C, respectiv... [2]

Deleted: 1.2

Moved (insertion) [2]

Formatted: Justified, Indent: First line: 0.5"

Deleted:

Formatted: Subscript

Formatted: Subscript

Deleted: 1

Deleted: This shift could be due to loss of small particles due to diffusion, coagulation, etc.

Deleted: f

Even when the chamber was clearly pressurized, our sensor was not sensitive enough to show a change in pressure. Chamber temperature started at room temperature (around 20 °C or slightly above) and increased to a maximum of 30 °C after 5 hours of use when all the UV lights were turned on, with most of the increase happening within the first hour (Smith et al., 2019). The temperature increase during photochemical aging can impact partitioning of the semivolatile components. The gas phase partitioning coefficient is temperature dependent though its value is only available for a limited number of semivolatile compounds. We did not measure the impact of temperature on partitioning of the semivolatile components, but it is possible that the observed change in optical properties during photochemical aging could in part be attributed to this effect.

Growth of aerosol particle inside the chamber was represented as a growth in the geometric mean diameter (GMD) of the size distribution as shown in Figure 1. Aerosol growth in the chamber was expected to be due to coagulation, diffusional losses of particles, and condensation of the gases into existing particles. It is evident from Figure 1 that growth was larger during photochemical aging conditions compared to the dark aging, indicating aerosol growth was due to condensation and subsequent chemical transformations. However, for flaming-dominated combustion, growth in GMD was the same during both dark and photochemical aging conditions indicating that there was no condensational growth in those experiments. The chamber cleaning procedure is described in the supplement material ST-1.

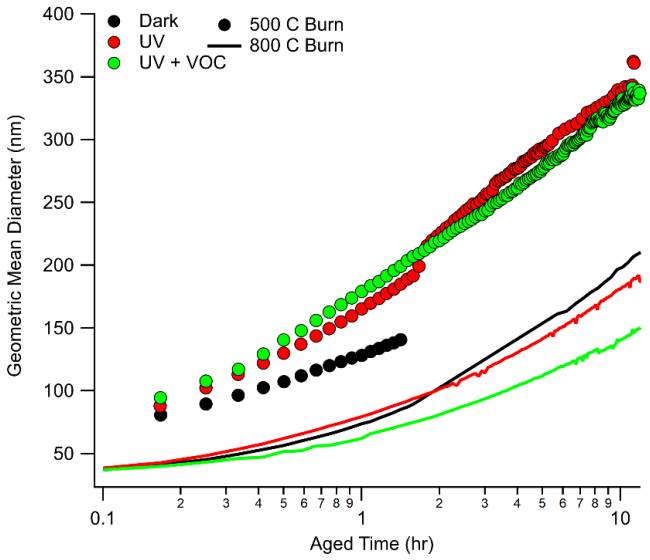

Figure 1: Growth of geometric mean diameter (GMD) as a function of photochemical age for eucalyptus under different burn and aged conditions represented in legend (black for dark aging, red for aging under light, and green for aging under light plus VOCs with solid line for flaming-dominated combustion and filled circle for smoldering-dominated combustion). Except for dark

Deleted: .
Deleted: .
Deleted: is
Deleted: for the
Deleted: is
Deleted: is
Deleted: for the
Deleted:
Formatted: Left
Formatted: Body Text, Left

aging conditions, zero time represent the time at which light is turn on. For the lower temperature case, initial GMD was typically about 85-90 nm whereas for higher temperature burn it was below 40 nm.

2.3 BB aerosol aging

2.3.1 Photochemical aging in a clean environment

For the purposes of these experiments, we define clean environment to be a smog chamber flushed out for 24 hours with clean air coming from the clean air generator. The only VOC's in the chamber came from the combustion of the fuel samples. Optical properties for fresh samples were measured using the procedure described below within 90 minutes of combustion, which allowed the size distribution of the aerosol to stabilize enough to conduct measurements without having a significant change in number density over the course of the experiment. For dark aging, the UV lights remained off, and measurements were repeated 12 hours after the introduction of BB aerosol in the chamber. For photochemical aging, a fresh sample was introduced into a clean chamber with the UV lights on immediately after combustion. Measurements were made after 12 hours of UV radiation.

2.3.2 Photochemical aging in a polluted environment

To study the effect of photochemical aging in a polluted environment, a mixture of VOCs was used to simulate an urban atmosphere. These VOCs were injected into the chamber and allowed to mix with the chamber air while the furnace heated up before the introduction of fuel samples. The rest of this section describes the preparation of this VOC mixture.

A high degree of accuracy is required in setting up the conditions of an experiment and performing subsequent measurements. All gas-phase measurements were traceable to an analytical balance (calibrated yearly), NIST-certified flow meter (Mesa Laboratories, model Definer 220, calibrated yearly), NIST-certified stopwatch, and/or certified gas standard. Sample introduction accounted for the NO_x produced from BB itself. Individual hydrocarbons and hydrocarbon mixtures were prepared with the analytical balance. These mixtures were composed of benzene (≥99.9%, Sigma-Aldrich), toluene (99.99%, Acros Organics), and ortho-xylene (99%, Alfa Aersar), and were prepared at the time of use. The concentration in molecules/cm^3 was determined consistently by measuring the mass of syringes before and after injection into the chamber. Using measured chamber pressure and temperature, the concentration in ppbv was estimated. All instruments were typically calibrated at the same time before a round of experimentation. NO and NO_2 were calibrated by passing certified standards through a calibrated MFC and mixing the standard with a calibrated flow of air in a ~30 mL glass mixing ball. Ozone was produced by passing air through an inline O_3 generator (UVP, model 97-0066-01). Using a calibrated NO_x instrument, the O_3 mixing ratio was determined by titrating it with NO to make NO_2. By measuring the O_3 signal, the calibration of O_3, in mV ppmv^{-1}, was performed.

Deleted:

Deleted: ... [3]

Deleted: 2

Deleted:

Deleted: 2

Deleted: o

Deleted: Optical properties were measured using the procedure described below soon after the chamber was well mixed

Formatted: Font:10 pt

Deleted: For the photochemical aging, a new burn was made, and the particles were kept in the chamber for 12 hours with the UV lights on

Deleted: 2

Deleted:

To represent a polluted urban environment, we used an emission inventory for urban environments from South Africa. This does not necessarily represent the east African emission inventory, but this does serve as a baseline, since it is the only available data to us for the continent. This data was obtained from the South African Air Quality Information System (SAAQIS) and included concentrations of NO_x, NO, NO_2, CO, O_3, benzene, toluene, ortho-xylene, and ethylbenzene for several South African sites (Diepkloof, Kliprivier, Three Rivers, Sharpeville, Sebokeng, Zamdela, Thabazimbi, Lephalalae, Phalaborwa, and Mokopnae). The VOC data was obtained from the two weeks (M-F) of July 11 – 15 and July 18 – 22, which was in the middle of the peak burning season for South Africa for the year 2016. The urban areas (Diepkloof and Kliprivier) had combined average mixing ratios of 1.16, 3.48, and 1.44 ppbv for benzene, toluene, and o-xylene, respectively. Suburban areas (Three Rivers, Sebokeng, and Zamdela) had combined average mixing ratios of 1.69, 4.02, and 0.70 ppbv for the aforementioned gases, respectively. Interestingly, suburban regions had somewhat higher average benzene and toluene mixing ratios, though o-xylene was only half the average urban concentration.

A mixture was prepared using equal by volumes of benzene, toluene, and o-xylene, and 2.5 mg of the mixture was injected by syringe into a U-shaped glass tube attached to the chamber. This resulted in a mixing ratio of 29.7, 24.9, and 21.9 ppbv for benzene, toluene, and o-xylene, respectively. The concentration injected into the chamber was approximately 7 – 26 times more concentrated than values found from urban South African emissions and 6 – 18 times more concentrated that suburban values. The reason for these elevated levels was mostly due to sample preparation constraints, since the amounts needed for an exact match were too small for our scale to weight appropriately. Concentrations in the chamber were intentionally higher than atmospheric conditions, in order to age the BB aerosol faster and accentuate the potential effect of SOA.

2.4 Optical properties measurement

Deleted: 3

BB aerosol was size selected for optical property measurements by passing the sample through an impactor inlet with a 710 µm nozzle (3.8 µm diameter cut point), charge neutralizer (TSI model 3081), and a long differential mobility analyzer (DMA) (TSI model 3080). Particles with mobility diameters centered at 200, 300, and 400 nm were selected by the DMA for this study. We verified that the standard deviations of the size distributions did not overlap (Poudel et al., 2017). The aerosol number density was measured by a water condensation particle counter (WCPC) (TSI model 3788), which was attached after the optical property instruments (shown in Figure 2) and provided flow through the entire setup at 0.58 sL min^{-1}. Further, the DMA and WCPC could be rearranged and combined to form an SMPS, which was used to determine size distributions before taking optical property measurements.

Deleted:

Deleted: .

Optical properties were measured using the extinction-minus-scattering technique (Weingartner et al., 2003;Bond et al., 1999;Sheridan et al., 2005), which uses CRDS to measure the total extinction of light and integrating sphere nephelometry to measure the scattering of light for the same aerosol sample (Moosmüller et al., 2005;Thompson et al., 2002;Thompson et al., 2008;Strawa et al., 2006). The details of the CRDS/Nephelometry optical properties measurement system is described in our recent work (Singh et al., 2014;Singh et al., 2016). A brief description is provided here. The extinction coefficient α_{ext} (m^{-1}) is $\geq$ 1 and is defined as:

Deleted:

$$\alpha_{ext} = \frac{R_L}{c_{air}}\left(\frac{1}{\tau} - \frac{1}{\tau_0}\right) = \sigma_{ext} N_{CRD} \quad (2)$$

where c_{air} is the speed of light in air, R_L is the ratio of mirror-to-mirror distance to the length of the cavity occupied by the sample, τ and τ_0 are the ring-down times, or the time it takes the light intensity to reach $1/e$ of the original intensity, of the sample and the blank measurement, respectively, σ_{ext} is the extinction cross-section of the aerosol in m^2, and N_{CRD} is the number concentration of the aerosol.

After being size selected, aerosol enter the ring-down cavity, where extinction was measured by passing a laser beam coupled to the cavity mode through the sample volume. The 355 nm beam from a Continuum Surelite I-20 Nd:YAG laser (at 20 Hz) pumps an optical parametric oscillator (OPO) laser, which can produce a range of wavelengths. For this study, we used a wavelength range of 500 to 570 nm and a single set of mirrors. Highly reflective mirrors confine most of the laser intensity within the CRDS, with a photomultiplier tube measuring the intensity of the light exiting the mirror after each round trip inside the cavity. Extinction is determined from the decay of light intensity exiting the mirrors. Our system allows measurement of optical properties at a wide range of wavelengths over most of the solar spectrum to determine "featured" extinction cross sections as a function of wavelength.

A purge flow of nitrogen was used to keep the mirrors clean. After the CRDS the aerosol enter the integrating nephelometer (TSI, model 3563), where scattering is measured at three wavelengths (centered at 453, 554, and 698 nm). Lastly, the number density of the particles was measured by the WCPC, as stated above. As previously reported by Singh et al. (2014), estimated particle losses in the CRDS are 14.2, 14.7, and 11.4% for 200, 300, and 400 nm particle sizes, respectively, and estimated losses in the nephelometer are 8.6, 7.1, and 6.3 % for the aforementioned sizes, respectively.

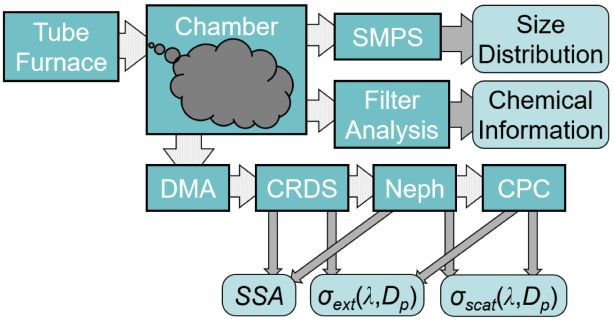

Figure 2: Scheme and flowchart for optical properties measurement

All flows, except the DMA sheath flow, are calibrated against a NIST-certified flow meter (Mesa Laboratories, model Definer 220) that is factory calibrated on a yearly basis and has a listed accuracy of < 1 %. Figure 2 describes the flowchart of the experiments.

2.5 Error analysis of optical properties measurements

In our previous work (Singh et al., 2014) we have comprehensively and holistically accounted for known sources of random and systematic errors and developed a statistical framework for including the contributions to

Deleted: .

Deleted: 4

random error. The combined extinction cross section uncertainty (10 − 11%) was largely dominated by CPC measurement error (10%). The calculation flow for determining the average extinction cross section (σ_{ext}), absorption cross section (σ_{abs}), and single scattering albedo (ω), was already described (Singh et al., 2014). The estimated uncertainties are 11%, 15%, and 2.1% for σ_{ext}, σ_{abs}, and ω, respectively.

The DMA can often allow multiply charged particles to pass through, that can result in artificially large measured cross sections, even for small number densities (Uin et al., 2011). Other groups have shown that measured extinction coefficients exceeded the predicted ones for 100 and 200 nm particles, which are most affected by the "multiple size–multiple charge" problem (Radney et al., 2009). As such, only particles 200 nm or greater were considered in this work. However, even with 200 nm particles, it has been shown that a small DMA sizing error can still produce significant changes in the extinction (Radney et al., 2013). In principle, errors in the DMA must be corrected (Miles et al., 2011;Toole et al., 2013). However, we did not make corrections due to DMA sizing error in this work but reported the percentage errors (the overestimation of SSA) caused by multiply charged particles for each aerosol size studied.

Deleted: work.

2.6 Aerosol chemical speciation monitor (ACSM)

Deleted: 5

An aerosol chemical speciation monitor (ACSM; Aerodyne Research Inc., USA) was used to measure the chemical composition of sub-micron non-refractive particulate mass. Details about the ACSM can be found elsewhere (Ng et al., 2011). Briefly, dry aerosol from the chamber was sampled into the ACSM through a critical aperture with a diameter of 100 µm at a flow rate of 85 mL min^{-1}. The recorded data was processed using the ACSM local toolkit (v.1.6.0.3) for Igor Pro. Since this work does not use mass loading in a quantitative way, we chose a collection efficiency of 1 for all species, similar to a previous study (Ng et al., 2011).

3 Results and discussion

3.1 Optical properties measurements.

Aerosol optical properties, namely scattering and extinction coefficient for size selected aerosol, were measured for three different east African biomass fuels. The selected fuels (eucalyptus, olive, and acacia) represent the most common trees in east Africa for domestic use, which contributes to significant aerosol loading. Each fuel was placed into the tube furnace at two different combustion temperatures. The term combustion temperature for this work represents the set temperatures of the furnace (initially heated at 500 ℃ and 800 ℃) to investigate the impact of ignition temperature on aerosol optical properties and chemical composition. In both cases, the furnace was allowed to reach the desired temperature before the sample was placed inside. In this paper, only the results from smoldering-dominated combustion under all aging conditions and the results of the fresh flaming-dominated combustion samples are reported. SSA values were measured for size selected particles having mobility diameters of 200, 300 and 400 nm.

Deleted: Each fuel was burned at two different combustion temperatures (500 °C and 800 °C) to investigate the impact of ignition temperature on aerosol optical properties and chemical composition. The optical properties of dark and photochemically aged aerosol were also measured

Deleted:

3.2 Impact of size on SSA

SSA was calculated by taking the ratio of scattering coefficient to the extinction coefficient measured for the wavelength range from 500 – 570 nm at 2.0 nm interval. Calibration of the system and the error analysis in the calculation of SSA from the experimental measurements is described in section 2.5. We calculated the scattering coefficients at the CRDS wavelength range by using the scattering angstrom exponent from the measured scattering coefficients.

Submicron aerosol show size dependent SSA values in visible wavelengths. Size-selected SSA values measured at 532nm in this study are compared with the size selected SSA valued calculated using Mie theory for two different refractive indices as shown in Figure 3. These refractive indices were proposed by Bond and Bergstrom, (2006) for BC and Levin et al. (2010) for smoldering biomass burning particles. While no pronounced size dependence was observed for aerosol from flaming-dominated combustion, contrary to what was predicted by Mie theory, the SSA did show size dependence for aerosol from smoldering-dominated combustion. This is due to the impact of multiply charged aerosol not discriminated by the DMA. Since we did not correct for the presence of multiply charged particles in this work, as described in section 2.5, this behavior was expected. The impact of multiply charged particles is more significant for flaming-dominated combustion (no pronounced size-dependent SSA) compared with the smoldering-dominated combustion (with some size-dependent SSA). This is a consequence of different particle size distributions. As shown in Figure S3, the presence of a second peak in the size distribution for flaming-dominated burns was expected to increase the impact of multiply charged particles on the observed SSA.

Recently, we estimated the impact of multiply charged particles on SSA using an Aerosol Particle Mass Analyzer (APM; Kanomax model 3602). We did not have this capability early in this study. APM was connected in-line after the DMA and subsequent optical properties were measured for freshly emitted aerosol. Details about the measurement strategy is given by Radney and Zangmeister (2016). It was found that, for smoldering-dominated burns, our SSA values were over estimated by a maximum of 8% for 200 and 300 nm sizes and by 5% for 400 nm size particles. Whereas, for flaming-dominated burns, our SSA values were overestimated by 12% for 200 and 300 nm sizes and by 9% for 400 nm size.

Deleted: 4

Deleted: -

Deleted: s

Deleted: calculated

Deleted: predicted

Deleted: by

Deleted: at 532 nm wavelength for both combustion temperatures as shown in

Formatted: Font:Not Bold

Deleted: Refractive indices (real and imaginary parts) were chosen to represent black and brown carbon samples based on values found

Formatted: Font:Not Bold

Deleted: .

Formatted: Font:Not Bold

Formatted: Font:Not Bold

Formatted: Font:Not Bold

Formatted: Font:Not Bold

Formatted: Font:Not Bold

Formatted: Normal, Indent: First line: 0", Pattern: Clear

Deleted: Figure 3 also shows the SSA of size-selected aerosol from different fuels combusted under different temperatures and the SSA of size-selected aerosol predicted from Mie theory. While no pronounced size dependence was observed for flaming-dominated aerosols, contrary to what was predicted by Mie theory, the SSA does show size dependence, for smoldering-dominated aerosols. This may be due to the impact of multiply charged aerosol not discriminated by the DMA. We did not make corrections due to multiply charged particles in this work as described in section 2.4. However, the impact of multiply charged particles on SSA is generally small for larger particles considered in this work, which have diameters of 300 or 400 nm. We have verified that the impact of multiply charged particle on SSA is low.

Deleted: This was done using an Aerosol Particle Mass analyzer APM (Kanomax APM 3602) in-line after the DMA and subsequent optical property measurements of freshly emitted BBA. Details about the measurement strategy is given by

Deleted: It was found that, due to the presence of multiply charged particles, our reported SSA values were overestimated by a maximum of 8% for 200 nm and 300 nm particles. ... [4]

Formatted: Pattern: Clear

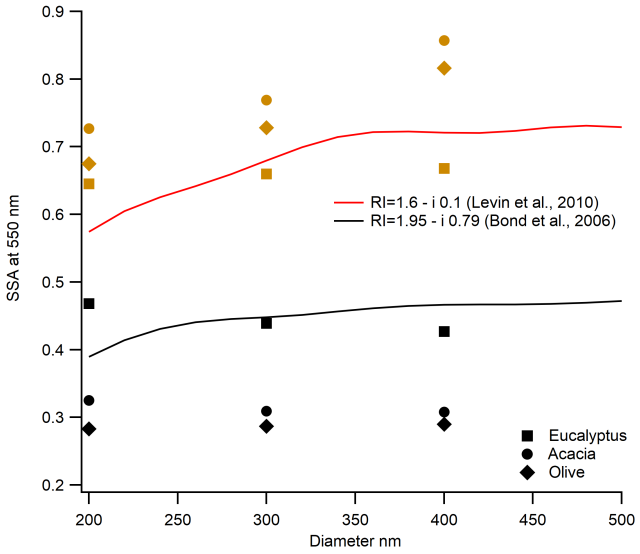

Figure 3: Impact of aerosol particle size on SSA. The solid red line is modeled SSA using Mie theory using refractive index from Levin et al. (2010), representing typical BB emission and black line is modeled SSA by Mie theory using refractive index from Bond et al. (2006), representing black carbon. Neither line is a fit to the data. Symbols are the different fuel types represented in the legend with black color for flaming-dominated combustion and brown color for smoldering-dominated combustion.

Formatted: Font:Bold

3.3 Single scattering albedo of freshly emitted aerosol

Figure 4 shows plot of SSA vs wavelength of light for freshly emitted 300 nm size aerosol from the different fuels at two different furnace temperatures (MCEs). The 200 and 400 nm particles show a similar behavior. The results show no wavelength dependence of SSA in the measured wavelength range of 500 −570 nm at both combustion temperatures. The dashed lines represent the propagated uncertainty (1 standard deviation) of the SSA, based on extinction and scattering coefficients. The extinction errors from the CRDS are mainly influenced by variability in the ring-down time. The SSA shows dependence on fuel type even under the same combustion condition. This was consistent for all particle sizes investigated.

Deleted: combustion

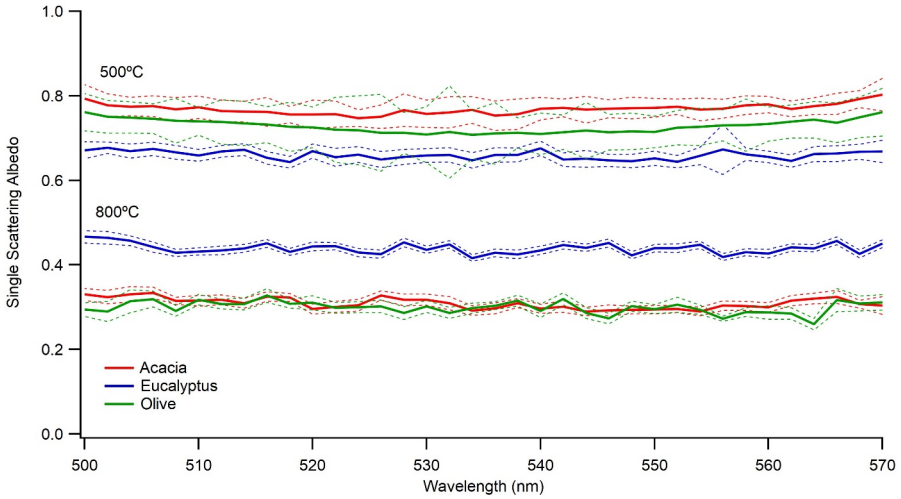

Figure 4: Single scattering albedo of 300 nm size-selected aerosol emitted at combustion temperatures of 500 °C and 800 °C. Solid blue, green, and red lines are for the average SSA from the three measurements and the dotted lines are the corresponding uncertainties (1 standard deviation) in the measured SSA.

The SSA values of the flaming-dominated combustion ranges from 0.287 to 0.439, whereas the SSA values of the smoldering-dominated combustion ranges from 0.66 to 0.769 for the different fuels. The average MCE for flaming-dominated combustion was 0.974 ± 0.015, while the average MCE for smoldering-dominated combustion was 0.878 ± 0.008. These MCE values suggest that at 800 °C combustion is flaming dominated which produces more BC, and at 500 °C combustion is smoldering dominated, which produces more OC (Christian et al., 2003;Ward et al., 1992). This explains the lower SSA values at higher combustion temperatures. A qualitative visual measure of the impacts of combustion temperature on aerosol properties can also be gleaned by looking at the color of the collected filter samples, as shown in Figure S4. As evident from Figure S4, flaming- dominated aerosol looks black, whereas smoldering-dominated aerosol looks brownish, indicating a visual difference between BC dominated and OC dominated emissions from the same fuel under different combustion temperatures.

The range of SSA for smoldering-dominated combustion was comparable to previous studies with similar MCE values (Liu et al., 2014;Pokhrel et al., 2016). On comparing the SSA of the three different fuels under two different combustion temperatures, it is apparent that SSA is controlled more by combustion condition rather than fuel type. Although there appeared to be a small but clear dependence of SSA on fuel type, there was a larger variation in SSA for the same fuel under two different combustion conditions, compared to the variation due to the inter fuel variability under the same combustion temperature. This result was consistent with a previous study, which showed that SSA is highly correlated with the ratio of elemental carbon to total carbon (proxy for the combustion condition),

Deleted: The range of SSA values for flaming-dominated combustion of different fuels is 0.287 to 0.439, whereas the range for the same fuels during smoldering-dominated combustion is 0.66 to 0.769. The average MCE for flaming-dominated combustion is 0.974 ± 0.015, while the average for smoldering-dominated combustion is 0.878 ± 0.008. These MCE values suggest that combustion at 800 °C is dominated by the flaming stage of combustion, which produces more BC, and combustion at 500 °C is dominated by the smoldering stage of combustion, which produces more OC

Deleted: T

Deleted: impact

Deleted: distinguished visually by

Deleted: 2

Deleted: 2

Deleted: is

Deleted: s

Deleted: i

Deleted: i

even for a wide variety of fuels (Pokhrel et al., 2016). A complete list of sizes selected SSA of different fuels measured at two combustion temperatures and under different aging conditions is provided in Table S1.

In the companion paper to this (Smith et al., 2020) methanol extracts from BB aerosol collected on Teflon filters were analyzed by ultra-performance liquid chromatography interfaced to both a diode array detector and an electrospray ionization high-resolution quadrupole time-of-flight mass spectrometer (UPLC/DAD-ESI-HR-QTOFMS) in negative ion mode. This was used to determine the relative abundance and light absorption properties of BB organic aerosol constituents. MS analysis of BB aerosol extracts from flaming-dominated combustion (Figure S5a and Table S2) revealed very little difference between the two fuel types, suggesting that there are either very few smoldering-dominated aerosol species produced for either fuel under these combustion conditions, or there are numerous species that are essentially the same between the samples. However, given that Eucalyptus has a higher SSA than Acacia, this would suggest that Eucalyptus has more non-absorbing OA, or at least less absorbing than BC. Since it was Acacia that appears to have many more low-abundant organic constituents, several possibilities exist to explain these differences in SSA, as explored in more depth in the companion paper (Smith et al., 2020). It is likely that Eucalyptus combustion products were not captured by some aspect of the extraction and UPLC/DAD-ESI-HR-QTOFMS analyses, that the observed differences in SSA are due to morphology differences, or some combination thereof. One potential explanation would be the presence of significant amounts of eucalyptol in the BB aerosol, which is a large fraction of Eucalyptus oil, and is a cyclic ester that lacks any basic functionality amiable for negative ion mode analysis, has good solubility in alcohols, and does not absorb in the UV and visible spectrum. An examination of the UV-visible spectra (Figure S6a) from the DAD shows no absorbing species in either region.

Chemical analysis revealed that for smoldering-dominated combustion, Eucalyptus and Acacia had a variety of compounds in common, such as lignin pyrolysis products, distillation products, and cellulose breakdown products (Figure S5b and Table S2). Several lignin pyrolysis products and distillation products are more prevalent in Eucalyptus than in Acacia, while pyrolysis products of cellulose and at least one nitroaromatic species were more prevalent in Acacia. Given that these lignin pyrolysis and distillation products are known chromophores and are more prevalent in Eucalyptus than in Acacia, while Acacia has a higher abundance of non-chromophores derived from sugars and cellulose, one would assume that Eucalyptus would be more absorbing (i.e. have a lower SSA) than Acacia in the visible spectrum. Despite the chemical analysis not capturing absolute amounts of OA, Acacia was found to have an SSA that is higher than Eucalyptus by 0.1 to 0.2, which is consistent with chemical measurements. This suggests that Acacia has either larger absolute amounts of non-chromophore compounds or Eucalyptus has a greater quantity of chromophores whose absorptive properties extend to the 500 – 570 nm region of the visible spectrum. An analysis of the chromatographically-integrated UV/Visible spectrum (Figure S6b) shows that there are chromophores whose absorption features peak near ~290 nm and extend into the 500 – 570 nm region, though a normalized spectrum does not appear to show drastic differences between species.

Figure 5 shows the SSA plotted as a function of MCE at 532 nm. Overall, our values of SSA agree well with the previous studies (Pokhrel et al., 2016;Liu et al., 2014) with some outliers. This could potentially be because we are comparing results for size-selected as opposed to bulk aerosol. In general, the variation of the SSA with MCE from the size-selected and bulk aerosol show a consistent behavior with higher SSA for the lower MCE cases and

Deleted: 2

Deleted: i

Deleted: 2

Deleted: 1

Deleted: .

Deleted: ar

lower SSA for higher MCE cases. As mentioned earlier, there occur some variabilities in SSA and MCE values even for the same combustion temperature. This could be due the dependence of SSA and MCE on fuel type or due to factors that we are not aware of. In general, however, combustion temperature plays a major role on the optical properties of the emitted aerosol. This suggests that by simply varying the combustion temperature, we can generate aerosols with very different optical properties and combustion efficiencies (Saleh et al., 2018;Liu et al., 2014).

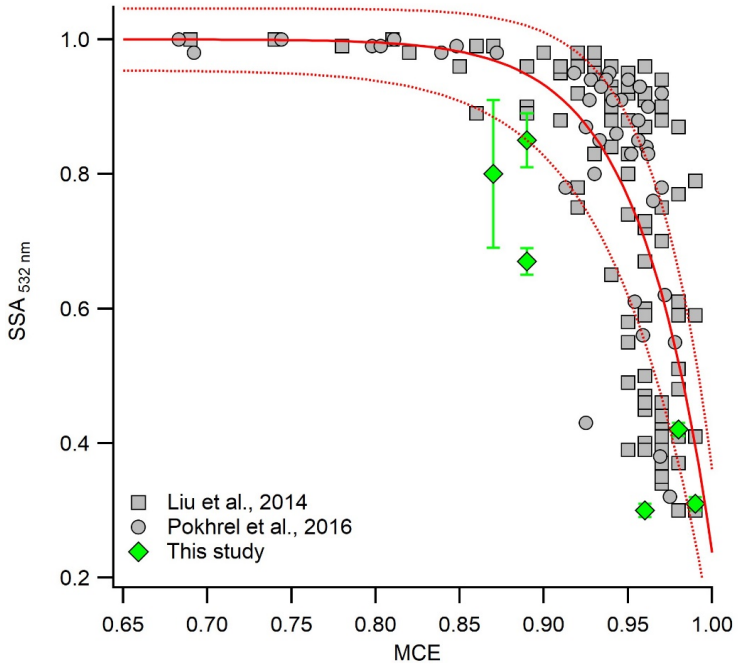

Figure 5: SSA of 400 nm size-selected aerosol at 532 nm as function of MCE under different combustion temperatures. Gray symbols are the SSA of bulk aerosol from previous studies (Liu et al., 2014; Pokhrel et al., 2016). Solid and dashed red lines are the best fit and the uncertainty bounds proposed by Liu et al. (2014).

3.4 Impact of dark aging on SSA

As BB aerosol age, their properties evolve due to competing chemical and physical processes (Hodshire et al., 2019;Yokelson et al., 2009;Akagi et al., 2012;Vakkari et al., 2018;Formenti et al., 2003;Garofalo et al., 2019). The particle dynamics was different in the dark compared to photochemical aging since there was a pronounced increase of particle size and density which was also observed in previous laboratory and ambient measurements (Reid et al., 1998;Zhang et al., 2011). We did not have the capability to measure density during this work, however Figure S1 provides the number density as a function of time for smoldering-dominated Acacia and Eucalyptus as they aged

Deleted: in
Deleted: y
Formatted: Font:Bold
Deleted: s
Deleted: its
Deleted: is
Deleted: at night
Deleted: is

in the dark. Even though the RH remained the same and low in our experiments, under high relative humidity conditions, heterogeneous reactions may be facilitated to produce more water soluble inorganic salts such as sulfates and nitrates (Shi et al., 2014). The first nighttime field analysis of BB plume intercepts for agricultural fuels showed that oxidation for rice straw and ponderosa pine was dominated by NO_3 (Decker et al., 2019). To simulate the impact of dark aging on aerosol optical properties, BB aerosol was aged in dark for 24 hours in absence of UV lights and additional ozone. The relative humidity in these experiments was very low (i.e. below the detection limit of our instrument). Optical properties of the freshly emitted aerosol were measured initially, with repeat measurements taken after the particles were left in the chamber to age in the dark. Figure 6 shows the impact of dark aging on SSA for the 300-nm size-selected aerosol emitted during smoldering-dominated combustion. Regardless of fuel type, there occurred an increase in SSA during aging with some fuel dependence, the largest of which was observed for olive. A two-tail T-test confirmed that increase in mean SSA is statistically significant for all three cases. The results are similar for the 200 nm and 400 nm particles as shown in Table S1.

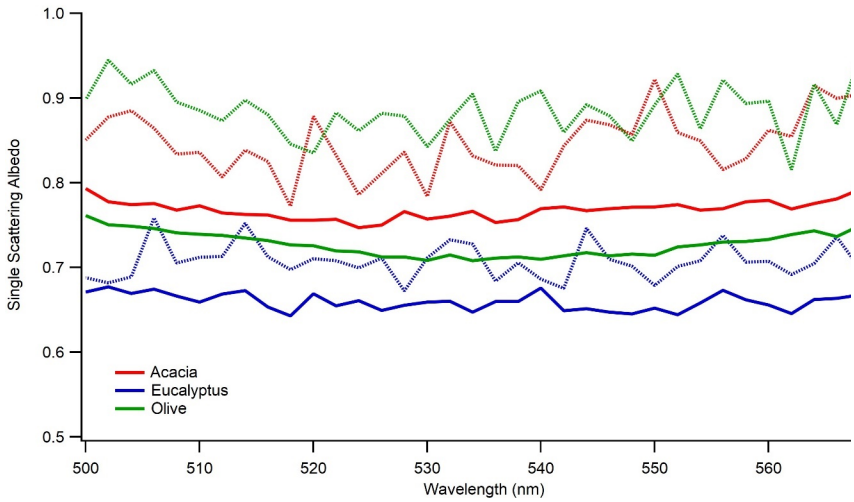

Figure 6: Impact of dark aging on SSA of 300 nm sized-selected aerosol emitted during smoldering-dominated combustion. Solid lines are for freshly emitted particle and dotted lines are for dark aged particles in the chamber. Different colors are for the different fuels listed in the legend.

Nighttime chemistry in BB studies is still unclear (Hodshire et al., 2019). The potential mechanism for the observed result could be due to the formation of less/non-absorbing secondary organic aerosol. To further explore the possibility of the observed increase in SSA, we looked at the scattering and extinction cross-section of the fresh and dark aged aerosol. Figure S7 shows the changes in extinction and scattering cross-section of 300 nm size particles emitted during smoldering-dominated combustion under dark aging. For all fuel types studied, there occurred a

Deleted: s

Deleted: rites

Deleted: BB aerosol was aged without UV lights on and kept overnight for 24 hours

Formatted: Font:Bold

Deleted: The potential mechanism for the observed result could be due to nighttime oxidation initiated by ozone or nitrate chemistry or the formation of less/non-absorbing secondary organic aerosol

Deleted: S3

significant increase in the scattering and extinction cross-section, indicating the occurrence of chemistry, even during dark aging. The increase in cross-section was driven by the scattering cross-section, with no significant change in absorption cross-section during aging. If a greater portion of the particle consisted of scattering SOA, one would expect a decrease in absorption cross-section if scattering cross-section of the particle increase for a given particle size, but this did not seem to be the case. While we did not characterize the chemical constituents of dark aged BBA in these experiments, there is a significant body of literature that has. (Li et al., 2015;Ramasamy et al., 2019;Hartikainen et al., 2018). Previous work by Tiitta et al. (2016) investigated dark and UV aging under several combustion conditions. It is not entirely clear which is equivalent to our smoldering-dominated combustion cases, given that their "slow ignition" produced significantly more VOCs when compared to their "fast ignition" experiments, but more hydrocarbon-like POA was produced from "fast ignition" experiments. These experiments were not distinguished by a combustion temperature and the MCE was not measured, but they were differentiated based on the amount of kindling used in their masonry heater. In either case, a significant amount of organonitrates were formed during dark aging via oxidation from NO_3 in the presence of ozone. Only in the slow ignition case was there a significant formation of SOA from ozonolysis during dark aging (~12% by mass from ozonolysis compared to ~12% from OH radical NO_3 and ~76% from and proxy radical based on positive matrix factorization analysis). A significant increase in the inorganic fraction of the aerosol was not expected given the low RH in these experiments (Li et al., 2015). Hartikainen et al. (2018) also observed significant formation of nitrogen-containing organic compounds in both particulate and gas phase during dark aging, with significant partitioning into the condensed phase. Little oxidation of the particulate phase was observed compared to photochemical aging. While these studies examined chemical transformations in the particulate and gas phases, they did not characterize the effects of these changes on optical properties. Given the increase in the scattering cross-section of the particles without altering the absorption cross-section observed in this work, one likely explanation is that smaller particle with high fractions of BC increase their mobility diameter upon SOA formation. This SOA, however, is partially absorbing, so that the expected decrease in absorption was not seen; or was at least mitigated to a change within uncertainty. While this absorption must extend to the 500 – 570 nm region of the spectrum, several nitro-aromatic species and functionalized PAHs are able to absorb at such long wavelengths (Fleming et al., 2020).

Unlike smoldering-dominated combustion, we were not able to track the aging of aerosol emitted during the flaming-dominated combustion due to some experimental issues. First, there was a significantly low aerosol emission due to more complete combustion of the fuel. For 300 nm and 400 nm size ranges, the number concentration of the particles emitted during flaming-dominated combustion was a factor of two to four lower than those emitted during smoldering-dominated combustion. In addition, due to the highly absorbing nature of the flaming-dominated aerosol, the scattering cross-section of the aerosol was significantly lower than that of the smoldering-dominated aerosol. Therefore, due to the very low number concentration and highly absorbing nature of the particles, the scattering coefficient of flaming-dominated aerosol was below the detection limit of our nephelometer during the aging experiments. Hence, we did not feel confident in reporting the SSA of dark aged particles emitted during flaming-dominated combustion. Figure S8 shows the impact of dark aging on the extinction cross-section of flaming-dominated aerosol. Even though a significant increase occurred in the extinction cross-sections during dark aging of

Deleted: oes

Deleted:

Deleted: is

Deleted: is

Deleted: is

Deleted: 4

Deleted: s

smoldering-dominated aerosol, we did not observe such behaviors during aging of flaming-dominated aerosol, indicating no significant changes in their optical properties. As shown in Figure S8b, there was a slight increase in the extinction cross-section for olive. However, when accounting a 12 % uncertainty in the cross-section, this increase in extinction cross-section is statistically insignificant. Since the extinction cross-section did not change between fresh and dark aged BBA of the same aerosol, it can be inferred that there was no change in the SSA during dark aging of flaming-dominated aerosol. This could potentially be due to limited emission of the nighttime oxidants and VOCs, unlike during smoldering-dominated combustion.

Deleted: .
Deleted: 4 (
Deleted:)
Deleted: is
Deleted: oes
Deleted: is

3.5 Impact of photochemical aging

To study the impact of photochemical aging on the optical properties of aerosol, we performed the aging of BB aerosol with the UV lights turned on. In addition, to simulate the impact of photochemical aging in a polluted environment, we added VOCs (benzene, toluene, and xylene) to mimic urban pollution as described in section 2.3.2. For both conditions, scattering and extinction coefficients were measured after 12 hours of aging in the chamber. Figure 7 shows the comparison of SSA from fresh and photochemically aged aerosol. As expected, there was an enhancement in the SSA of photochemically aged aerosol. A key point to mention is that fresh and aged SSA were from two different burns and we confirmed that under the same burn conditions the SSA of the same fuels remain within the measurement uncertainties of our instruments. Since this study used size-selected aerosols, the increase in SSA was only possible if the particles became less absorbing because of aging, which could potentially be due to the formation of non-absorbing secondary organic aerosol during photochemical aging. An increase in SSA is possible during photochemical aging due to degradation in brown carbon absorptivity (Sumlin et al., 2017) but the impact of brown carbon on SSA in mid-visible wavelength is small (Pokhrel et al., 2016). BrC components undergo photochemical transformations during atmospheric transport, including photobleaching or photoenhancement of their absorption coefficients. For example, the field studies of Forrister et al. (2015) and Selimovic et al. (2018) observed a substantial decay in aerosol UV light absorption in biomass burning plumes corresponding to a half-life of 9 to 15 hours. Recent laboratory and field studies suggested that OH oxidation in the atmosphere may alter the optical properties of BrC, leading to absorption enhancement or bleaching (Schnitzler and Abbatt, 2018;Sumlin et al., 2017;Dasari et al., 2019). These studies were made at wavelengths of 375 and 405 nm, while ours were done in the visible range, so they are not directly applicable to this work. As evident from Figure 7, after 12 hours of aging, the BB aerosol becomes highly scattering, leading to SSA values of greater than 0.9 in the mid-visible wavelengths, even though fresh BB aerosol were highly absorbing, with SSA below 0.8.

Deleted: s
Deleted: .2
Deleted: s
Deleted: a
Deleted: is
Deleted: However, t
Deleted: wavelength of light
Deleted: .

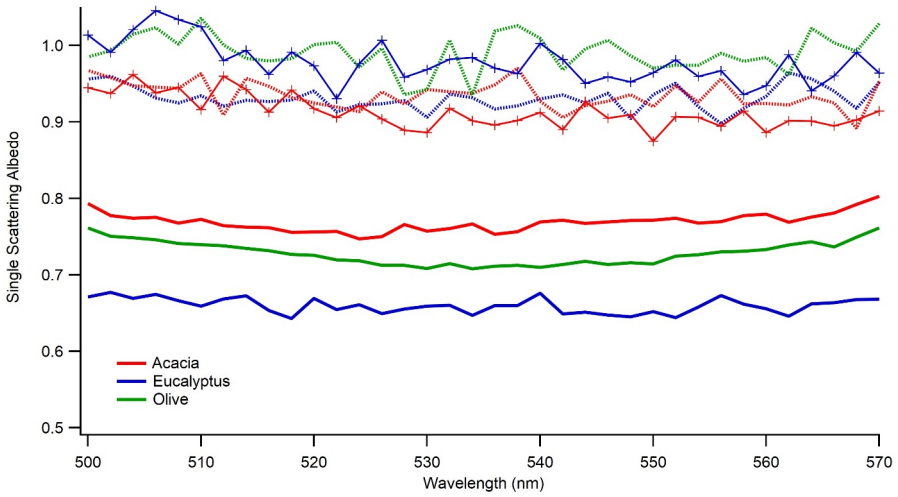

Figure 7: Impact of photochemical aging (light and light plus VOC) on SSA of 300 nm size selected smoldering-dominated aerosols. Solid lines are for freshly emitted particles, dotted lines are for aging under the light, and solid lines with symbols are for aging under light plus VOCs. Different colors are for the different fuels listed in the legend.

Despite the use of anthropogenic VOCs with concentrations larger than those average values found in urban and suburban regions of South Africa, no distinct effect was observed for SSA values of BB aerosol produced during smoldering-dominated combustion. This is most likely because we took our measurements after 12 hours of aging, which was enough time for the scattering nature of the SOA produced during aging to drive measured SSA values to unity, regardless of the chemical pathway taken due to the addition of VOCs. While it is possible that the relatively long aging time could obscure some of the effects due to the presence of VOCs, it is also possible that molecular species are dominated by combustion products, and the effects of additional VOCs are insignificant. The later would suggest that the three-aromatic species representing anthropogenic pollutants do not seem to affect the optical properties of BB aerosol. Another possibility would be that high NOx concentrations would prevent the formation of ozone, which would hinder SOA formation from aromatic species. Indeed, examining the effects of aging on the chemical composition of BB aerosol (Figure S9 and Tables S3 and S4) shows very few species that could be attributed to anthropogenic VOCs; specifically, only dihydroxyphthalic acid produced from xylene. For both Eucalyptus and Acacia, an isomer of dihydroxybenzene, such as resorcinol or catechol, was removed to the highest degree from the fresh BB aerosol upon photochemical aging. Generally, very few compounds were produced to a significant extent, and both fuels were dominated by a loss of chromatophoric lignin pyrolysis and distillation products. This includes a great number of functionalized benzaldehyde, benzoic acid, and coumarin species. Not surprisingly, the associated absorbance from these chromophores, mostly from 200 – 350 nm, was also attenuated with respect to age (Figure S10). This may be caused in part by the photo-bleaching effect created by the irradiation of UV light for 12 hours,

Formatted: Font:Bold

Deleted: dominate molecular species

Deleted:

Deleted: The later would suggest that anthropogenic pollution does not seem to affect the optical properties of BB aerosol

heterogeneous OH oxidation, and SOA formation of non-chromophores. It would seem that molecular absorption extends to the mid visible region of the spectrum, as evidenced by its negative and non-zero slope of absorption vs. wavelength in the 500-570 nm region. This corresponded well with absorption cross section measurements of 300 nm particles and the comparison holds when the comparison was made in terms of an Ångstrom absorption exponent. Additionally, photochemical aging produces more absorption at longer wavelengths, which results in a negative Ångstrom absorption exponent and a positive slope in this region. This could be due to the production or persistence of compounds that absorb at such long wavelengths, such as nitro-aromatic species, where one isomer that is either nitroanisole, nitrocresol, or possibly nitrobenzyl alcohol was observed in mass spectra, and functionalized PAHs, where dihydroxyanthracene was observed to be produced; likely from the oxidation of anthracene.

This fact suggests that a study with higher temporal resolution is needed to simulate the impact of the VOCs on aerosol SSA, where continuous or much more frequent measurements are needed to determine the impact of urban pollution on aerosol SSA. Such a study, using continuous measurements, is not possible for our setup when particles are also size selected. Like dark aged conditions, we were not able to estimate SSA for flaming-dominated combustion due to the low particle concentration and highly absorbing nature of the aerosol. A chemical analysis of aged BB aerosol produced at this temperature revealed very few changes, suggesting that only a few molecular species were produced by combustion at this temperature.

During aging, the size distribution of the particles was measured every 5 minutes using an SMPS. To account for the impact of additional VOCs on secondary aerosol formation, we estimated the OA enhancement from the time series of an SMPS spectra during these experiments. This was done by applying a fixed wall loss rate constant as estimated in our previous study (Smith et al., 2019) and assuming a similar loss rate for POA vs SOA. We also assumed that OA is the major aerosol fraction emitted during smoldering-dominated combustion. In addition, we also made an assumption of constant density during aging, which gave us the lower estimate of the OA enhancement because the density of the aerosol increases with age compared to POA (Tkacik et al., 2017). The OA enhancement calculation method used in this study was based on the work by Saleh et al. (2013). Briefly, we applied the wall loss time constant to estimate the potential decrease in the OA mass loading only due to wall loss based on the OA mass before the lights were turned on. The OA enhancement factor was estimated by taking the ratio of measured aerosol mass to the predicted aerosol mass based on the wall loss rate constant. It was shown that partitioning of vapors to walls in laboratory experiments may alter apparent SOA production (Hodshire et al., 2019). For the particle wall loss rates used in this work, we did not correct for partitioning of vapors to walls, which was not generally negligible (Krechmer et al., 2016). Furthermore, it was shown that the tubing between the tube furnace and smog chamber might create loss in the gas phase precursors for SOA formation (Pagonis et al., 2017;Deming et al., 2019;Liu et al., 2019). Relatively greater losses of particles with increased length of sampling tubes was observed (Kumar et al., 2008). Our connecting tubing was short enough (0.5 m) to neglect such a loss. Figure S11 shows the time series of OA enhancement during different aging conditions. We did not observe a distinct difference between the OA enhancement factors under light aged and light plus VOC aged cases. This could potentially be due to our assumptions and the uncertainty related to the SMPS where the uncertainty in the particle count by the WCPC is ±10%. Previous field and modeling studies found significant enhancement in the SOA formation due to impact of urban pollution (Shrivastava et al., 2019). This

Deleted: molecular

Deleted: is

Deleted: a

Deleted: is

Deleted: 5

Formatted: Font:10 pt, Not Italic

Deleted: .

Formatted: Font:10 pt, Not Italic

Formatted: Font:Not Italic

fact also suggests that we need more rigorous study to simulate impact of urban pollution of secondary aerosol formation in the laboratory.

Although as an ACSM was not available early in this study, we designed an experiment to compare the performance of the OA enhancement calculation based on the SMPS with the ACSM during a separate burn. As mentioned earlier, we used a first order decay of the POA based on the estimated wall loss rate constant from the chamber characterization experiments. Figure S12 shows the comparison of OA enhancement using the ACSM OA mass loading vs the estimated submicron aerosol mass based on the SMPS. In general, the trend of OA enhancement is similar but the SMPS seems to underestimate the actual OA enhancement compared to the ACSM. The difference between the OA enhancement estimated by ACSM and SMPS was within 10%, indicating that estimated OA enhancement lies within the SMPS uncertainty range.

4 Conclusions

Biomass burning is the major source of atmospheric primary particles and vapors, which are precursors for secondary aerosol. BB aerosol have been extensively studied through both field and laboratory environments for North American fuels to understand the changes in optical and chemical properties as a function of aging. There is a clear research need for a wider sampling of fuels from different regions of the world for laboratory studies. This work is such an attempt to study the optical and chemical properties of fuels common in east Africa and represents the first such study.

The existence of significant variability in the observed field and laboratory measurements has been reviewed recently (Hodshire et al., 2019). While laboratory studies provide control over environmental and chemical conditions to study aging by controlling one variable at a time, it may not necessarily recreate atmospheric conditions in atmospheric plumes in the field. Differences in fuel mixture and fuel conditions, such as moisture content, can lead to different emissions. There is a difference in dilution rates between field studies, which is variable, and laboratory studies, which are not variable. Other differences include temperature differences, background OA concentrations, and wall losses. Despite the gap in reconciling field and laboratory studies, some limited comparisons can be made.

For fresh emissions, SSA showed no pronounced size dependence for flaming-dominated combustion, whereas same size dependence was observed for smoldering-dominated combustion. This may be due to the impact of multiply charged aerosol, which is not discriminated by the DMA. For the wavelength range used in this study, no wavelength dependence of SSA was observed under all conditions. However, SSA showed dependence on fuel type in general, even under the same combustion conditions.

In general, combustion temperature plays a major role in the optical properties of the emitted aerosol. In all cases the measured SSA values for flaming-dominated combustion were in the range between 0.287 and 0.439, indicating highly absorbing aerosol, which corresponds to aerosol dominated by black carbon. We observed a large increase in the SSA during smoldering-dominated combustion, which was in the range between 0.66 and 0.769. Under the same combustion conditions and airflow, there was a clear dependence of SSA on fuel type, with eucalyptus

Deleted: 6

Deleted: is

Deleted:

Deleted: s

Deleted: s

Deleted: s

Deleted: are

Deleted: to

Deleted: is

Deleted: to

Deleted:

Deleted: is

producing aerosol with higher SSA values than olive and acacia. However, these variations are relatively small, indicating that the SSA was more controlled by the combustion conditions than the fuel type.

Negative mode UPLC/DAD-ESI-HR-QTOFMS analyses of fresh BBA from flaming-dominated combustion suggest that there was some chemical constituent that was not being captured by this analysis. Given that Eucalyptus has a higher SSA than Acacia for the flaming-dominated combustion this would indicate that Eucalyptus has more non-absorbing OA that was not observed by chemical analysis, such as the presence of eucalyptol. Smoldering-dominate combustion of Eucalyptus and Acacia produced a variety of compounds in common, such as lignin pyrolysis products, distillation products, and cellulose breakdown products. Several lignin pyrolysis products and distillation products were more prevalent in Eucalyptus than in Acacia, while pyrolysis products of cellulose and at least one nitroaromatic species were more prevalent in Acacia. This is consistent with the higher SSA of Acacia when compared to Eucalyptus for the smoldering-dominated combustion, since lignin pyrolysis products and distillation products are known chromophores, while compounds derived from sugars and cellulose are non-chromophores.

Regardless of fuel types, there occurred an increase in SSA during dark aging, with some fuel dependence, the largest of which was observed for smoldering-dominated aerosol emitted from olive. A significant increase in the scattering and extinction cross-section (mostly dominated by scattering) was observed, indicating the occurrence of chemistry, even during dark aging. Based on the relevant literature, we hypothesize that nitrogen-containing secondary organic aerosol is formed during dark aging (Li et al., 2015;Hartikainen et al., 2018;Nguyen et al., 2011;Tiitta et al., 2016) . It is possible that this SOA is absorbing in this region, which was offsetting the effect of an increasing OA fraction with age. A chemical analysis of dark aged aerosol during these experiments is planned for future work, and should allow us to test this theory.

After 12 hours of photochemical aging, BB aerosol becomes highly scattering with SSA values above 0.9, even though fresh emissions were more absorbing with SSA below 0.8. This can be attributed to oxidation in the chamber.

Due to the very low number concertation of flaming-dominated aerosols, the results were inconclusive, and we plan to conduct measurements by increasing the amount of fuel burned. We also attempted to simulate polluted urban environments by injecting anthropogenic VOCs into the chamber, but no distinct difference was observed. An examination of the chemical composition of aged BBA shows very few species that could be attributed to anthropogenic VOCs. Generally, very few compounds were produced to a significant extent, and both fuels were dominated by a loss of chromatophoric lignin pyrolysis and distillation products, likely caused by a combination of photo-bleaching, heterogeneous OH oxidation, and SOA formation of non-chromophores. No significant OA enhancement was observed because of the VOC injection either, even though significantly enhanced SOA formation was observed in polluted environments (Shrivastava et al., 2019;Shrivastava et al., 2015). This suggests a need for more rigorous controlled time dependent measurements.

To our knowledge, this is the first laboratory study of optical properties of east African biomass fuels for domestic use. Ongoing work includes systematic study of optical properties using six different African fuels as a function of aging, burn conditions, VOC concentration, and RH.

Deleted: is

Deleted: is

Deleted: is

Deleted: is

Deleted: are

Deleted: is

Author contribution: Damon Smith conducted the experiments and analyzed the data; Marc Fiddler and Solomon Bililign designed the experiments and contributed to writing and editing. Rudra Pokhrel contributed to the data analysis and interpretation.

Competing interests: The authors declare that they have no conflict of interest.

References

Akagi, S. K., Craven, J. S., Taylor, J. W., McMeeking, G. R., Yokelson, R. J., Burling, I. R., Urbanski, S. P., Wold, C. E., Seinfeld, J. H., Coe, H., Alvarado, M. J., and Weise, D. R.: Evolution of trace gases and particles emitted by a chaparral fire in California, Atmos. Chem. Phys., 12, 1397-1421, 10.5194/acp-12-1397-2012, 2012.

Andreae, M. O., and Merlet, P.: Emission of trace gases and aerosols from biomass burning, Global Biogeochemical Cycles, 15, 955-966, 10.1029/2000GB001382, 2001.

Babar, Z. B., Park, J.-H., Kang, J., and Lim, H.-J.: Characterization of a Smog Chamber for Studying Formation and Physicochemical Properties of Secondary Organic Aerosol, Aerosol and Air Quality Research, 16, 3102-3113, 10.4209/aaqr.2015.10.0580, 2016.

Bahadur, R., Praveen, P. S., Xu, Y., and Ramanathan, V.: Solar absorption by elemental and brown carbon determined from spectral observations, Proceedings of the National Academy of Sciences, 109, 17366-17371, 10.1073/pnas.1205910109, 2012.

Bank, W.: More People Have Access to Electricity Than Ever Before, but World Is Falling Short of Sustainable Energy Goals, in, 2019.

Bond, T. C., Anderson, T. L., and Campbell, D.: Calibration and intercomparison of filter-based measurements of visible light absorption by aerosols, Aerosol Science and Technology, 30, 582-600, 10.1080/027868299304435, 1999.

Bond, T. C., Streets, D. G., Yarber, K. F., Nelson, S. M., Woo, J.-H., and Klimont, Z.: A technology-based global inventory of black and organic carbon emissions from combustion, Journal of Geophysical Research: Atmospheres, 109, n/a-n/a, 10.1029/2003JD003697, 2004.

Bond, T. C., Bhardwaj, E., Dong, R., Jogani, R., Jung, S., Roden, C., Streets, D. G., and Trautmann, N. M.: Historical emissions of black and organic carbon aerosol from energy-related combustion, 1850–2000, Global Biogeochemical Cycles, 21, n/a-n/a, 10.1029/2006GB002840, 2007.

Bond, T. C., Zarzycki, C., Flanner, M. G., and Koch, D. M.: Quantifying immediate radiative forcing by black carbon and organic matter with the Specific Forcing Pulse, Atmos. Chem. Phys., 11, 1505-1525, 10.5194/acp-11-1505-2011, 2011.

Boucher, O., D. Randall, P. Artaxo, C. Bretherton, G. Feingold, P. Forster, V.-M. Kerminen, Y. Kondo, H. Liao, U. Lohmann, P. Rasch, S.K. Satheesh, S. Sherwood, B. Stevens and X.Y. Zhang: Clouds and Aerosols, in: Climate Change 2013: The Physical Science Basis. Contribution of Working Group I to the Fifth Assessment Report of the Intergovernmental Panel on Climate Change, edited by: Stocker, T. F., D. Qin, G.-K. Plattner, M. Tignor, S.K. Allen, J. Boschung, A. Nauels, Y. Xia, V. Bex and P.M. Midgley Cambridge University Press, Cambridge, United Kingdom and New York, NY, USA., 2013.

Brown, H., Liu, X., Feng, Y., Jiang, Y., Wu, M., Lu, Z., Wu, C., Murphy, S., and Pokhrel, R.: Radiative effect and climate impacts of brown carbon with the Community Atmosphere Model (CAM5), Atmos. Chem. Phys., 18, 17745-17768, 10.5194/acp-18-17745-2018, 2018.

Bruns, E. A., El Haddad, I., Slowik, J. G., Kilic, D., Klein, F., Baltensperger, U., and Prévôt, A. S. H.: Identification of significant precursor gases of secondary organic aerosols from residential wood combustion, Scientific Reports, 6, 27881, 10.1038/srep27881
https://www.nature.com/articles/srep27881 - supplementary-information, 2016.

Christian, T. J., Kleiss, B., Yokelson, R. J., Holzinger, R., Crutzen, P. J., Hao, W. M., Saharjo, B. H., and Ward, D. E.: Comprehensive laboratory measurements of biomass-burning emissions: 1. Emissions from Indonesian, African, and other fuels, Journal of Geophysical Research-Atmospheres, 108, 10.1029/2003jd003704, 2003.

Chung, C. E., Ramanathan, V., and Decremer, D.: Observationally constrained estimates of carbonaceous aerosol radiative forcing, Proceedings of the National Academy of Sciences, 109, 11624-11629, 10.1073/pnas.1203707109, 2012.

Crutzen, P., and Andreae, M.: Biomass Burning in the Tropics: Impact on Atmospheric Chemistry and Biogeochemical Cycles, Science (New York, N.Y.), 250, 1669-1678, 10.1126/science.250.4988.1669, 1991.

Dasari, S., Andersson, A., Bikkina, S., Holmstrand, H., Budhavant, K., Satheesh, S., Asmi, E., Kesti, J., Backman, J., Salam, A., Bisht, D. S., Tiwari, S., Hameed, Z., and Gustafsson, Ö.: Photochemical degradation affects the light absorption of water-soluble brown carbon in the South Asian outflow, Science Advances, 5, eaau8066, 10.1126/sciadv.aau8066, 2019.

Decker, Z. C. J., Zarzana, K. J., Coggon, M., Min, K.-E., Pollack, I., Ryerson, T. B., Peischl, J., Edwards, P., Dubé, W. P., Markovic, M. Z., Roberts, J. M., Veres, P. R., Graus, M., Warneke, C., de Gouw, J., Hatch, L. E., Barsanti, K. C., and Brown, S. S.: Nighttime Chemical Transformation in Biomass Burning Plumes: A Box Model Analysis Initialized with Aircraft Observations, Environmental Science & Technology, 53, 2529-2538, 10.1021/acs.est.8b05359, 2019.

Delfino, R. J., Brummel, S., Wu, J., Stern, H., Ostro, B., Lipsett, M., Winer, A., Street, D. H., Zhang, L., Tjoa, T., and Gillen, D. L.: The relationship of respiratory and cardiovascular hospital admissions to the southern California wildfires of 2003, Occupational and Environmental Medicine, 66, 189-197, 10.1136/oem.2008.041376, 2009.

Deming, B. L., Pagonis, D., Liu, X., Day, D. A., Talukdar, R., Krechmer, J. E., Gouw, J. A. d., Jimenez, J. L., and Ziemann, P. J.: Measurements of Delays of Gas-Phase Compounds in a Wide Variety of Tubing Materials due to Gas–wall Interactions, Atmos. Meas. Tech., 12, 3453, 2019.

Eck, T. F., Holben, B. N., Ward, D. E., Dubovik, O., Reid, J. S., Smirnov, A., Mukelabai, M. M., Hsu, N. C., O'Neill, N. T., and Slutsker, I.: Characterization of the optical properties of biomass burning aerosols in Zambia during the 1997 ZIBBEE field campaign, Journal of Geophysical Research: Atmospheres, 106, 3425-3448, 10.1029/2000JD900555, 2001.

Edwards, D. P., Emmons, L. K., Gille, J. C., Chu, A., Attié, J. L., Giglio, L., Wood, S. W., Haywood, J., Deeter, M. N., Massie, S. T., Ziskin, D. C., and Drummond, J. R.: Satellite-observed pollution from Southern Hemisphere biomass burning, Journal of Geophysical Research: Atmospheres, 111, n/a-n/a, 10.1029/2005JD006655, 2006.

Elliott, C. T., Henderson, S. B., and Wan, V.: Time series analysis of fine particulate matter and asthma reliever dispensations in populations affected by forest fires, Environmental Health, 12, 11, 10.1186/1476-069X-12-11, 2013.

Feng, Y., Ramanathan, V., and Kotamarthi, V.: Brown carbon: A significant atmospheric absorber of solar radiation, ATMOSPHERIC CHEMISTRY AND PHYSICS, 13, 8607-8621, 10.5194/acp-13-8607-2013, 2013.

Fleming, L. T., Lin, P., Roberts, J. M., Selimovic, V., Yokelson, R., Laskin, J., Laskin, A., and Nizkorodov, S. A.: Molecular composition and photochemical lifetimes of brown carbon chromophores in biomass burning organic aerosol, Atmos. Chem. Phys., 20, 1105-1129, 10.5194/acp-20-1105-2020, 2020.

Formenti, P., Elbert, W., Maenhaut, W., Haywood, J., Osborne, S., and Andreae, M.: Inorganic and carbonaceous aerosols during the Southern African Regional Science Initiative (SAFARI 2000) experiment: Chemical characteristics, physical properties, and emission data for smoke from African biomass burning, Journal of Geophysical Research: Atmospheres, 108, https://doi.org/10.1029/2002jd002408, 2003.

Forrister, H., Liu, J., Scheuer, E., Dibb, J., Ziemba, L., Thornhill, K. L., Anderson, B., Diskin, G., Perring, A. E., and Schwarz, J. P.: Evolution of Brown Carbon in Wildfire Plumes, Geophys. Res. Lett., 42, 4623, 2015.

Forster, P., Ramaswamy, V., Artaxo, P., Berntsen, T., Betts, R., Fahey, D., Haywood, J., Lean, J., Lowe, D., Myhre, G., Nganga, J., Prinn, R., Raga, G., Schulz, M., Dorland, R., Bodeker, G., Boucher, O., Collins, W., Conway, T., and Whorf, T.: Changes in Atmospheric Constituents and in Radiative Forcing, in, 2007.

Garofalo, L. A., Pothier, M. A., Levin, E. J. T., Campos, T., Kreidenweis, S. M., and Farmer, D. K.: Emission and Evolution of Submicron Organic Aerosol in Smoke from Wildfires in the Western United States, ACS Earth Space Chem., 3, 1237, 2019.

Hartikainen, A., Yli-Pirilä, P., Tiitta, P., Leskinen, A., Kortelainen, M., Orasche, J., Schnelle-Kreis, J., Lehtinen, K. E. J., Zimmermann, R., Jokiniemi, J., and Sippula, O.: Volatile Organic Compounds from Logwood Combustion: Emissions and Transformation under Dark and Photochemical Aging Conditions in a Smog Chamber, Environmental Science & Technology, 52, 4979-4988, 10.1021/acs.est.7b06269, 2018.

Henderson, S. B., Brauer, M., MacNab, Y. C., and Kennedy, S. M.: Three Measures of Forest Fire Smoke Exposure and Their Associations with Respiratory and Cardiovascular Health Outcomes in a Population-Based Cohort, Environmental Health Perspectives, 119, 1266-1271, doi:10.1289/ehp.1002288, 2011.

Hennigan, C. J., Miracolo, M. A., Engelhart, G. J., May, A. A., Presto, A. A., Lee, T., Sullivan, A. P., McMeeking, G. R., Coe, H., Wold, C. E., Hao, W. M., Gilman, J. B., Kuster, W. C., de Gouw, J., Schichtel, B. A., Collett Jr, J. L., Kreidenweis, S. M., and Robinson, A. L.: Chemical and physical transformations of organic aerosol from the photo-oxidation of open biomass burning emissions in an environmental chamber, Atmos. Chem. Phys., 11, 7669-7686, 10.5194/acp-11-7669-2011, 2011.

Hodshire, A. L., Akherati, A., Alvarado, M. J., Brown-Steiner, B., Jathar, S. H., Jimenez, J. L., Kreidenweis, S. M., Lonsdale, C. R., Onasch, T. B., Ortega, A. M., and Pierce, J. R.: Aging Effects on Biomass Burning Aerosol Mass and Composition: A Critical Review of Field and Laboratory Studies, Environmental Science & Technology, 53, 10007-10022, 10.1021/acs.est.9b02588, 2019.

Hodzic, A., Madronich, S., Bohn, B., Massie, S., Menut, L., and Wiedinmyer, C.: Wildfire particulate matter in Europe during summer 2003: meso-scale modeling of smoke emissions, transport and radiative effects, Atmos. Chem. Phys., 7, 4043-4064, 10.5194/acp-7-4043-2007, 2007.

Holstius, D. M., Reid, C. E., Jesdale, B. M., and Morello-Frosch, R.: Birth Weight following Pregnancy during the 2003 Southern California Wildfires, Environmental Health Perspectives, 120, 1340-1345, doi:10.1289/ehp.1104515, 2012.

Hungershoefer, K., Zeromskiene, K., Iinuma, Y., Helas, G., Trentmann, J., Trautmann, T., Parmar, R., Wiedensohler, A., Andreae, M., and Schmid, O.: Modelling the optical properties of fresh biomass burning aerosol produced in a smoke chamber: results from the EFEU campaign, Atmospheric Chemistry and Physics, 8, 3427-3439, https://doi.org/10.5194/acp-8-3427-2008, 2008.

Ichoku, C., Giglio, L., Wooster, M. J., and Remer, L. A.: Global characterization of biomass-burning patterns using satellite measurements of fire radiative energy, Remote Sensing of Environment, 112, 2950-2962, https://doi.org/10.1016/j.rse.2008.02.009, 2008.

IPCC: IPCC Fifth Assessment Report, Climate Change 2013: The Physical Science Basis, 2014.

Jacobson, M. Z.: A physically-based treatment of elemental carbon optics: Implications for global direct forcing of aerosols, Geophysical Research Letters, 27, 217-220, 10.1029/1999GL010968, 2000.

Johnston, F., Hanigan, I., Henderson, S., Morgan, G., and Bowman, D.: Extreme air pollution events from bushfires and dust storms and their association with mortality in Sydney, Australia 1994–2007, Environmental Research, 111, 811-816, https://doi.org/10.1016/j.envres.2011.05.007, 2011.

Johnston, F. H., Henderson, S. B., Chen, Y., Randerson, J. T., Marlier, M., DeFries, R. S., Kinney, P., Bowman, D. M. J. S., and Brauer, M.: Estimated Global Mortality Attributable to Smoke from Landscape Fires, Environmental Health Perspectives, 120, 695-701, doi:10.1289/ehp.1104422, 2012.

Kirchstetter, T. W., Novakov, T., and Hobbs, P. V.: Evidence that the spectral dependence of light absorption by aerosols is affected by organic carbon, Journal of Geophysical Research: Atmospheres, 109, doi:10.1029/2004JD004999, 2004.

Klimont, Z., Cofala, J., Xing, J., Wei, W., Zhang, C., Wang, S., Kejun, J., Bhandari, P., Mathur, R., Purohit, P., Rafaj, P., Chambers, A., Amann, M., and Hao, J.: Projections of SO2, NOx and carbonaceous aerosols emissions in Asia, Tellus B, 61, 602-617, 10.1111/j.1600-0889.2009.00428.x, 2009.

Klimont, Z., Smith, S. J., and Cofala, J.: The last decade of global anthropogenic sulfur dioxide: 2000–2011 emissions, Environmental Research Letters, 8, 014003, 2013.

Koch, D., Menon, S., Genio, A. D., Ruedy, R., Alienov, I., and Schmidt, G. A.: Distinguishing Aerosol Impacts on Climate over the Past Century, Journal of Climate, 22, 2659-2677, 10.1175/2008jcli2573.1, 2009.

Krechmer, J. E., Pagonis, D., Ziemann, P. J., and Jimenez, J. L.: Quantification of Gas-Wall Partitioning in Teflon Environmental Chambers Using Rapid Bursts of Low-Volatility Oxidized Species Generated in Situ, Environ. Sci. Technol., 50, 5757, 2016.

Kumar, P., Fennell, P., Symonds, J., and Britter, R.: Treatment of losses of ultrafine aerosol particles in long sampling tubes during ambient measurements, Atmospheric Environment, 42, 8819-8826, https://doi.org/10.1016/j.atmosenv.2008.09.003, 2008.

Lamarque, J. F., Bond, T. C., Eyring, V., Granier, C., Heil, A., Klimont, Z., Lee, D., Liousse, C., Mieville, A., Owen, B., Schultz, M. G., Shindell, D., Smith, S. J., Stehfest, E., Van Aardenne, J., Cooper, O. R., Kainuma, M., Mahowald, N., McConnell, J. R., Naik, V., Riahi, K., and van Vuuren, D. P.: Historical (1850–2000) gridded anthropogenic and biomass burning emissions of reactive gases and aerosols: methodology and application, Atmos. Chem. Phys., 10, 7017-7039, 10.5194/acp-10-7017-2010, 2010.

Laskin, A., Laskin, J., and Nizkorodov, S. A.: Chemistry of Atmospheric Brown Carbon, Chemical Reviews, 115, 4335-4382, 10.1021/cr5006167, 2015.

Leskinen, A., Yli-Pirilä, P., Kuuspalo, K., Sippula, O., Jalava, P., Hirvonen, M. R., Jokiniemi, J., Virtanen, A., Komppula, M., and Lehtinen, K. E. J.: Characterization and testing of a new environmental chamber, Atmos. Meas. Tech., 8, 2267-2278, 10.5194/amt-8-2267-2015, 2015.

Levin, E. J. T., McMeeking, G. R., Carrico, C. M., Mack, L. E., Kreidenweis, S. M., Wold, C. E., Moosmüller, H., Arnott, W. P., Hao, W. M., Collett, J. L., and Malm, W. C.: Biomass burning smoke aerosol properties measured during Fire Laboratory at Missoula Experiments (FLAME), Journal of Geophysical Research: Atmospheres, 115, D18210, 10.1029/2009JD013601, 2010.

Li, C., Ma, Z., Chen, J., Wang, X., Ye, X., Wang, L., Yang, X., Kan, H., Donaldson, D. J., and Mellouki, A.: Evolution of biomass burning smoke particles in the dark, Atmospheric Environment, 120, 244-252, https://doi.org/10.1016/j.atmosenv.2015.09.003, 2015.

Liousse, C., Guillaume, B., Grégoire, J. M., Mallet, M., Galy, C., Pont, V., Akpo, A., Bedou, M., Castéra, P., Dungall, L., Gardrat, E., Granier, C., Konaré, A., Malavelle, F., Mariscal, A., Mieville, A., Rosset, R., Serça, D., Solmon, F., Tummon, F., Assamoi, E., Yobouć, V., and Van Velthoven, P.: Updated African biomass burning emission inventories in the framework of the AMMA-IDAF program, with an evaluation of combustion aerosols, Atmos. Chem. Phys., 10, 9631-9646, 10.5194/acp-10-9631-2010, 2010.

Liousse, C., Assamoi, E., Criqui, P., Granier, C., and Rosset, R.: Explosive growth in African combustion emissions from 2005 to 2030, Environmental Research Letters, 9, 035003, https://doi.org/10.1088/1748-9326/9/3/035003, 2014.

Liu, S., Aiken, A. C., Arata, C., Dubey, M. K., Stockwell, C. E., Yokelson, R. J., Stone, E. A., Jayarathne, T., Robinson, A. L., DeMott, P. J., and Kreidenweis, S. M.: Aerosol single scattering albedo dependence on biomass

combustion efficiency: Laboratory and field studies, Geophysical Research Letters, 41, 742-748, 10.1002/2013GL058392, 2014.

Liu, X., Huey, L. G., Yokelson, R. J., Selimovic, V., Simpson, I. J., Müller, M., Jimenez, J. L., Campuzano-Jost, P., Beyersdorf, A. J., and Blake, D. R.: Airborne Measurements of Western US Wildfire Emissions: Comparison with Prescribed Burning and Air Quality Implications, J. Geophys. Res. D: Atmos., 122, 6108, 2017.

Liu, X., Deming, B., Pagonis, D., Day, D. A., Palm, B. B., Talukdar, R., Roberts, J. M., Veres, P. R., Krechmer, J. E., Thornton, J. A., de Gouw, J. A., Ziemann, P. J., and Jimenez, J. L.: Effects of gas–wall interactions on measurements of semivolatile compounds and small polar molecules, Atmos. Meas. Tech., 12, 3137-3149, 10.5194/amt-12-3137-2019, 2019.

Ma, X., Yu, F., and Luo, G.: Aerosol direct radiative forcing based on GEOS-Chem-APM and uncertainties, Atmos. Chem. Phys., 12, 5563-5581, 10.5194/acp-12-5563-2012, 2012.

Mack, L. A., Levin, E. J. T., Kreidenweis, S. M., Obrist, D., Moosmüller, H., Lewis, K. A., Arnott, W. P., McMeeking, G. R., Sullivan, A. P., Wold, C. E., Hao, W. M., Collett Jr, J. L., and Malm, W. C.: Optical closure experiments for biomass smoke aerosols, Atmos. Chem. Phys., 10, 9017-9026, 10.5194/acp-10-9017-2010, 2010.

Mack, L. E.: Cavity Ring-Down Sectroscopy and the Retrieval of Aerosol Optical Properties from Biomass Burning During Flame 2, Master's, Colorado State University, CO, USA, 2008.

Malavelle, F., Pont, V., Mallet, M., Solmon, F., Johnson, B., Leon, J.-F., and Liousse, C.: Simulation of aerosol radiative effects over West Africa during DABEX and AMMA SOP-0, Journal of Geophysical Research: Atmospheres, 116, n/a-n/a, 10.1029/2010JD014829, 2011.

McMeeking, G. R., Kreidenweis, S. M., Baker, S., Carrico, C. M., Chow, J. C., Collett, J. L., Hao, W. M., Holden, A. S., Kirchstetter, T. W., Malm, W. C., Moosmüller, H., Sullivan, A. P., and Wold, C. E.: Emissions of trace gases and aerosols during the open combustion of biomass in the laboratory, Journal of Geophysical Research: Atmospheres, 114, D19210, 10.1029/2009JD011836, 2009.

Miles, R. E. H., Rudić, S., Orr-Ewing, A. J., and Reid, J. P.: Sources of Error and Uncertainty in the Use of Cavity Ring Down Spectroscopy to Measure Aerosol Optical Properties, Aerosol Science and Technology, 45, 1360-1375, 10.1080/02786826.2011.596170, 2011.

Moosmüller, H., Varma, R., and Arnott, W. P.: Cavity Ring-Down and Cavity-Enhanced Detection Techniques for the Measurement of Aerosol Extinction, Aerosol Science and Technology, 39, 30-39, 10.1080/027868290903880, 2005.

Naeher, L. P., Brauer, M., Lipsett, M., Zelikoff, J. T., Simpson, C. D., Koenig, J. Q., and Smith, K. R.: Woodsmoke Health Effects: A Review, Inhalation Toxicology, 19, 67-106, 10.1080/08958370600985875, 2007.

Ng, N. L., Herndon, S. C., Trimborn, A., Canagaratna, M. R., Croteau, P. L., Onasch, T. B., Sueper, D., Worsnop, D. R., Zhang, Q., Sun, Y. L., and Jayne, J. T.: An Aerosol Chemical Speciation Monitor (ACSM) for Routine Monitoring of the Composition and Mass Concentrations of Ambient Aerosol, Aerosol Science and Technology, 45, 780-794, 10.1080/02786826.2011.560211, 2011.

Nguyen, T. B., Laskin, J., Laskin, A., and Nizkorodov, S. A.: Nitrogen-Containing Organic Compounds and Oligomers in Secondary Organic Aerosol Formed by Photooxidation of Isoprene, Environmental Science & Technology, 45, 6908-6918, 10.1021/es201611n, 2011.

Pagonis, D., Krechmer, J. E., Gouw, J., Jimenez, J. L., and Ziemann, P. J.: Effects of Gas–wall Partitioning in Teflon Tubing and Instrumentation on Time-Resolved Measurements of Gas-Phase Organic Compounds, Atmos. Meas. Tech., 10, 4687, 2017.

Paulsen, D., Dommen, J., Kalberer, M., Prévôt, A. S. H., Richter, R., Sax, M., Steinbacher, M., Weingartner, E., and Baltensperger, U.: Secondary Organic Aerosol Formation by Irradiation of 1,3,5-Trimethylbenzene−NOx−H2O in a

New Reaction Chamber for Atmospheric Chemistry and Physics, Environmental Science & Technology, 39, 2668-2678, 10.1021/es0489137, 2005.

Pokhrel, R. P., Wagner, N. L., Langridge, J. M., Lack, D. A., Jayarathne, T., Stone, E. A., Stockwell, C. E., Yokelson, R. J., and Murphy, S. M.: Parameterization of single-scattering albedo (SSA) and absorption Ångström exponent (AAE) with EC / OC for aerosol emissions from biomass burning, Atmos. Chem. Phys., 16, 9549-9561, 10.5194/acp-16-9549-2016, 2016.

Poudel, S., Fiddler, M., Smith, D., Flurchick, K., and Bililign, S.: Optical properties of biomass burning aerosols: Comparison of experimental measurements and T-Matrix calculations, Atmosphere, 8, 228, https://doi.org/10.3390/atmos8110228, 2017.

Radney, J. G., Bazargan, M. H., Wright, M. E., and Atkinson, D. B.: Laboratory Validation of Aerosol Extinction Coefficient Measurements by a Field-Deployable Pulsed Cavity Ring-Down Transmissometer, Aerosol Science and Technology, 43, 71-80, 10.1080/02786820802482536, 2009.

Radney, J. G., Ma, X., Gillis, K. A., Zachariah, M. R., Hodges, J. T., and Zangmeister, C. D.: Anal. Chem., 85, 8319, 2013.

Radney, J. G., and Zangmeister, C. D.: Practical limitations of aerosol separation by a tandem differential mobility analyzer–aerosol particle mass analyzer, Aerosol Science and Technology, 50, 160-172, 10.1080/02786826.2015.1136733, 2016.

Ramasamy, S., Nakayama, T., Imamura, T., Morino, Y., Kajii, Y., and Sato, K.: Investigation of dark condition nitrate radical- and ozone-initiated aging of toluene secondary organic aerosol: Importance of nitrate radical reactions with phenolic products, Atmospheric Environment, 219, 117049, https://doi.org/10.1016/j.atmosenv.2019.117049, 2019.

Rappold, A. G., Stone, S. L., Cascio, W. E., Neas, L. M., Kilaru, V. J., Carraway, M. S., Szykman, J. J., Ising, A., Cleve, W. E., Meredith, J. T., Vaughan-Batten, H., Deyneka, L., and Devlin, R. B.: Peat Bog Wildfire Smoke Exposure in Rural North Carolina Is Associated with Cardiopulmonary Emergency Department Visits Assessed through Syndromic Surveillance, Environmental Health Perspectives, 119, 1415-1420, doi:10.1289/ehp.1003206, 2011.

Reid, J. S., Hobbs, P. V., Ferek, R. J., Blake, D. R., Martins, J. V., Dunlap, M. R., and Liousse, C.: Physical, Chemical, and Optical Properties of Regional Hazes Dominated by Smoke in Brazil, J. Geophys. Res., 103, 32059, 1998.

Roberts, G., Wooster, M. J., and Lagoudakis, E.: Annual and diurnal african biomass burning temporal dynamics, Biogeosciences, 6, 849-866, 10.5194/bg-6-849-2009, 2009.

Roberts, G. J., and Wooster, M. J.: Fire Detection and Fire Characterization Over Africa Using Meteosat SEVIRI, IEEE Transactions on Geoscience and Remote Sensing, 46, 1200-1218, 10.1109/TGRS.2008.915751, 2008.

Saleh, R., Robinson, E. S., Tkacik, D. S., Ahern, A. T., Liu, S., Aiken, A. C., Sullivan, R. C., Presto, A. A., Dubey, M. K., Yokelson, R. J., Donahue, N. M., and Robinson, A. L.: Brownness of organics in aerosols from biomass burning linked to their black carbon content, Nature Geoscience, 7, 647-650, 10.1038/ngeo2220, 2014.

Saleh, R., Marks, M., Heo, J., Adams, P. J., Donahue, N. M., and Robinson, A. L.: Contribution of brown carbon and lensing to the direct radiative effect of carbonaceous aerosols from biomass and biofuel burning emissions, Journal of Geophysical Research: Atmospheres, 120, 10,285-210,296, 10.1002/2015jd023697, 2015.

Saleh, R., Cheng, Z., and Atwi, K.: The Brown–Black Continuum of Light-Absorbing Combustion Aerosols, Environmental Science & Technology Letters, 5, 508-513, 10.1021/acs.estlett.8b00305, 2018.

Schnitzler, E. G., and Abbatt, J. P. D.: Heterogeneous OH oxidation of secondary brown carbon aerosol, Atmos. Chem. Phys., 18, 14539-14553, 10.5194/acp-18-14539-2018, 2018.

Schultz, M. G., Heil, A., Hoelzemann, J. J., Spessa, A., Thonicke, K., Goldammer, J. G., Held, A. C., Pereira, J. M. C., and van het Bolscher, M.: Global wildland fire emissions from 1960 to 2000, Global Biogeochemical Cycles, 22, GB2002, 10.1029/2007GB003031, 2008.

Schwarz, J. P., Spackman, J. R., Fahey, D. W., Gao, R. S., Lohmann, U., Stier, P., Watts, L. A., Thomson, D. S., Lack, D. A., Pfister, L., Mahoney, M. J., Baumgardner, D., Wilson, J. C., and Reeves, J. M.: Coatings and their enhancement of black carbon light absorption in the tropical atmosphere, Journal of Geophysical Research: Atmospheres, 113, n/a-n/a, 10.1029/2007JD009042, 2008.

Selimovic, V., Yokelson, R. J., Warneke, C., Roberts, J. M., Gouw, J., Reardon, J., and Griffith, D. W. T.: Aerosol Optical Properties and Trace Gas Emissions by PAX and OP-FTIR for Laboratory-Simulated Western US Wildfires during FIREX, Atmos. Chem. Phys., 18, 2929, 2018.

Sheridan, P. J., Arnott, W. P., Ogren, J. A., Andrews, E., Atkinson, D. B., Covert, D. S., Moosmuller, H., Petzold, A., Schmid, B., Strawa, A. W., Varma, R., and Virkkula, A.: The Reno Aerosol Optics Study: An evaluation of aerosol absorption measurement methods, Aerosol Science and Technology, 39, 1-16, 10.1080/027868290901891, 2005.

Shi, Y., Chen, J., Hu, D., Wang, L., Yang, X., and Wang, X.: Airborne submicron particulate (PM1) pollution in Shanghai, China: Chemical variability, formation/dissociation of associated semi-volatile components and the impacts on visibility, Science of The Total Environment, 473-474, 199-206, https://doi.org/10.1016/j.scitotenv.2013.12.024, 2014.

Shrivastava, M., Easter, R. C., Liu, X., Zelenyuk, A., Singh, B., Zhang, K., Ma, P. L., Chand, D., Ghan, S., and Jimenez, J. L.: Global Transformation and Fate of SOA: Implications of Low-Volatility SOA and Gas-Phase Fragmentation Reactions, J. Geophys. Res. D: Atmos., 120, 4169, 2015.

Shrivastava, M., Andreae, M. O., Artaxo, P., Barbosa, H. M. J., Berg, L. K., Brito, J., Ching, J., Easter, R. C., Fan, J., Fast, J. D., Feng, Z., Fuentes, J. D., Glasius, M., Goldstein, A. H., Alves, E. G., Gomes, H., Gu, D., Guenther, A., Jathar, S. H., Kim, S., Liu, Y., Lou, S., Martin, S. T., McNeill, V. F., Medeiros, A., de Sá, S. S., Shilling, J. E., Springston, S. R., Souza, R. A. F., Thornton, J. A., Isaacman-VanWertz, G., Yee, L. D., Ynoue, R., Zaveri, R. A., Zelenyuk, A., and Zhao, C.: Urban pollution greatly enhances formation of natural aerosols over the Amazon rainforest, Nature Communications, 10, 1046, 10.1038/s41467-019-08909-4, 2019.

Singh, S., Fiddler, M. N., Smith, D., and Bililign, S.: Error Analysis and Uncertainty in the Determination of Aerosol Optical Properties Using Cavity Ring-Down Spectroscopy, Integrating Nephelometry, and the Extinction-Minus-Scattering Method, Aerosol Science and Technology, 48, 1345-1359, 10.1080/02786826.2014.984062, 2014.

Singh, S., Fiddler, M. N., and Bililign, S.: Measurement of size-dependent single scattering albedo of fresh biomass burning aerosols using the extinction-minus-scattering technique with a combination of cavity ring-down spectroscopy and nephelometry, Atmos. Chem. Phys., 16, 13491-13507, 10.5194/acp-16-13491-2016, 2016.

Smith, D. M., Fiddler, M. N., Sexton, K. G., and Bililign, S.: Construction and Characterization of an Indoor Smog Chamber for Measuring the Optical and Physicochemical Properties of Aging Biomass Burning Aerosols, Aerosol and Air Quality Research, 19, 467-483, 10.4209/aaqr.2018.06.0243, 2019.

Smith, D. M., Cui, T., Fiddler, M. N., Pokhrel, R., Surratt, J. D., and Bililign, S.: Laboratory studies of fresh and aged biomass burning aerosols emitted from east African biomass fuels - Part 2: Chemical properties and characterization, Atmos. Chem. Phys. Discuss., 2020, 1-30, 10.5194/acp-2019-1160, 2020.

Smith, K. R., and Pillarisetti, A.: Household Air Pollution from Solid Cookfuels and Its Effects on Health., in: Injury Prevention and Environmental Health. 3rd edition, edited by: CN, M., Nugent R, and O, K., The International Bank for Reconstruction and Development / The World Bank;, Washington (DC), 2017.

Spracklen, D. V., Mickley, L. J., Logan, J. A., Hudman, R. C., Yevich, R., Flannigan, M. D., and Westerling, A. L.: Impacts of climate change from 2000 to 2050 on wildfire activity and carbonaceous aerosol concentrations in the western United States, Journal of Geophysical Research: Atmospheres, 114, 10.1029/2008jd010966, 2009.

Stefanidou, M., Athanaselis, S., and Spiliopoulou, C.: Health Impacts of Fire Smoke Inhalation, Inhalation Toxicology, 20, 761-766, 10.1080/08958370801975311, 2008.

Stier, P., Seinfeld, J. H., Kinne, S., Feichter, J., and Boucher, O.: Impact of nonabsorbing anthropogenic aerosols on clear-sky atmospheric absorption, Journal of Geophysical Research: Atmospheres, 111, n/a-n/a, 10.1029/2006JD007147, 2006.

Strawa, A. W., Elleman, R., Hallar, A. G., Covert, D., Ricci, K., Provencal, R., Owano, T. W., Jonsson, H. H., Schmid, B., Luu, A. P., Bokarius, K., and Andrews, E.: Comparison of in situ aerosol extinction and scattering coefficient measurements made during the Aerosol Intensive Operating Period, Journal of Geophysical Research: Atmospheres, 111, n/a-n/a, 10.1029/2005JD006056, 2006.

Streets, D. G., Bond, T. C., Lee, T., and Jang, C.: On the future of carbonaceous aerosol emissions, Journal of Geophysical Research: Atmospheres, 109, n/a-n/a, 10.1029/2004JD004902, 2004.

Sumlin, B. J., Pandey, A., Walker, M. J., Pattison, R. S., Williams, B. J., and Chakrabarty, R. K.: Atmospheric Photooxidation Diminishes Light Absorption by Primary Brown Carbon Aerosol from Biomass Burning, Environmental Science & Technology Letters, 4, 540-545, 10.1021/acs.estlett.7b00393, 2017.

Sumlin, B. J., Heinson, Y. W., Shetty, N., Pandey, A., Pattison, R. S., Baker, S., Hao, W. M., and Chakrabarty, R. K.: UV–Vis–IR spectral complex refractive indices and optical properties of brown carbon aerosol from biomass burning, Journal of Quantitative Spectroscopy and Radiative Transfer, 206, 392-398, https://doi.org/10.1016/j.jqsrt.2017.12.009, 2018.

Sutherland, E. R., Make, B. J., Vedal, S., Zhang, L., Dutton, S. J., Murphy, J. R., and Silkoff, P. E.: Wildfire smoke and respiratory symptoms in patients with chronic obstructive pulmonary disease, Journal of Allergy and Clinical Immunology, 115, 420-422, 10.1016/j.jaci.2004.11.030, 2005.

Thompson, J. E., Smith, B. W., and Winefordner, J. D.: Monitoring Atmospheric Particulate Matter through Cavity Ring-Down Spectroscopy, Analytical Chemistry, 74, 1962-1967, 10.1021/ac0110505, 2002.

Thompson, J. E., Barta, N., Policarpio, D., and DuVall, R.: A fixed frequency aerosol albedometer, Opt. Express, 16, 2191-2205, 10.1364/OE.16.002191, 2008.

Tiitta, P., Leskinen, A., Hao, L., Yli-Pirilä, P., Kortelainen, M., Grigonyte, J., Tissari, J., Lamberg, H., Hartikainen, A., Kuuspalo, K., Kortelainen, A. M., Virtanen, A., Lehtinen, K. E. J., Komppula, M., Pieber, S., Prévôt, A. S. H., Onasch, T. B., Worsnop, D. R., Czech, H., Zimmermann, R., Jokiniemi, J., and Sippula, O.: Transformation of logwood combustion emissions in a smog chamber: formation of secondary organic aerosol and changes in the primary organic aerosol upon daytime and nighttime aging, Atmos. Chem. Phys., 16, 13251-13269, 10.5194/acp-16-13251-2016, 2016.

Tkacik, D. S., Robinson, E. S., Ahern, A., Saleh, R., Stockwell, C., Veres, P., Simpson, I. J., Meinardi, S., Blake, D. R., and Yokelson, R. J.: A Dual-Chamber Method for Quantifying the Effects of Atmospheric Perturbations on Secondary Organic Aerosol Formation from Biomass Burning Emissions: Investigation of Biomass Burning SOA, J. Geophys. Res. D: Atmos., 122, 6043, 2017.

Toole, J. R., Renbaum-Wolff, L., and Smith, G. D.: A Calibration Technique for Improving Refractive Index Retrieval from Aerosol Cavity Ring-Down Spectroscopy, Aerosol Science and Technology, 47, 955-965, 10.1080/02786826.2013.805875, 2013.

Uin, J., Tamm, E., and Mirme, A.: Very Long DMA for the Generation of the Calibration Aerosols in Particle Diameter Range up to 10 µm by Electrical Separation, Aerosol and Air Quality Research, 11, 531-538, 10.4209/aaqr.2011.05.0068, 2011.

UN: World Population Prospects: The 2010 Revision, Comprehensive Tables. ST/ESA/SER.A/313., United Nations, Department of Economic and Social Affairs, Population Division, 2011.

Vakkari, V., Beukes, J. P., Dal Maso, M., Aurela, M., Josipovic, M., and van Zyl, P. G.: Major Secondary Aerosol Formation in Southern African Open Biomass Burning Plumes, Nat. Geosci., 11, 580, 2018.

van der Werf, G. R., Randerson, J. T., Giglio, L., Collatz, G. J., Mu, M., Kasibhatla, P. S., Morton, D. C., DeFries, R. S., Jin, Y., and van Leeuwen, T. T.: Global fire emissions and the contribution of deforestation, savanna, forest, agricultural, and peat fires (1997–2009), Atmos. Chem. Phys., 10, 11707-11735, 10.5194/acp-10-11707-2010, 2010.

Wang, X., Liu, T., Bernard, F., Ding, X., Wen, S., Zhang, Y., Zhang, Z., He, Q., Lü, S., Chen, J., Saunders, S., and Yu, J.: Design and characterization of a smog chamber for studying gas-phase chemical mechanisms and aerosol formation, Atmos. Meas. Tech., 7, 301-313, 10.5194/amt-7-301-2014, 2014.

Ward, D. E., Susott, R. A., Kauffman, J. B., Babbitt, R. E., Cummings, D. L., Dias, B., Holben, B. N., Kaufman, Y. J., Rasmussen, R. A., and Setzer, A. W.: Smoke and fire characteristics for cerrado and deforestation burns in Brazil: BASE-B Experiment, Journal of Geophysical Research: Atmospheres, 97, 14601-14619, 10.1029/92jd01218, 1992.

Weingartner, E., Saathoff, H., Schnaiter, M., Streit, N., Bitnar, B., and Baltensperger, U.: Absorption of light by soot particles: Determination of the absorption coefficient by means of aethalometers, Journal of Aerosol Science, 34, 1445-1463, 10.1016/s0021-8502(03)00359-8, 2003.

Williams, J. E., Weele, M. v., Velthoven, P. F. J. v., Scheele, M. P., Liousse, C., and Werf, G. R. v. d.: The Impact of Uncertainties in African Biomass Burning Emission Estimates on Modeling Global Air Quality, Long Range Transport and Tropospheric Chemical Lifetimes, Atmosphere, 3, 132, 2012.

Yang, M., Howell, S. G., Zhuang, J., and Huebert, B. J.: Attribution of aerosol light absorption to black carbon, brown carbon, and dust in China – interpretations of atmospheric measurements during EAST-AIRE, Atmos. Chem. Phys., 9, 2035-2050, 10.5194/acp-9-2035-2009, 2009.

Yokelson, R. J., Crounse, J. D., DeCarlo, P. F., Karl, T., Urbanski, S., Atlas, E., Campos, T., Shinozuka, Y., Kapustin, V., Clarke, A. D., Weinheimer, A., Knapp, D. J., Montzka, D. D., Holloway, J., Weibring, P., Flocke, F., Zheng, W., Toohey, D., Wennberg, P. O., Wiedinmyer, C., Mauldin, L., Fried, A., Richter, D., Walega, J., Jimenez, J. L., Adachi, K., Buseck, P. R., Hall, S. R., and Shetter, R.: Emissions from biomass burning in the Yucatan, Atmos. Chem. Phys., 9, 5785-5812, 10.5194/acp-9-5785-2009, 2009.

Yokelson, R. J., Burling, I. R., Gilman, J. B., Warneke, C., Stockwell, C. E., de Gouw, J., Akagi, S. K., Urbanski, S. P., Veres, P., Roberts, J. M., Kuster, W. C., Reardon, J., Griffith, D. W. T., Johnson, T. J., Hosseini, S., Miller, J. W., Cocker Iii, D. R., Jung, H., and Weise, D. R.: Coupling field and laboratory measurements to estimate the emission factors of identified and unidentified trace gases for prescribed fires, Atmos. Chem. Phys., 13, 89-116, 10.5194/acp-13-89-2013, 2013.

Zhang, H., Hu, D., Chen, J., Ye, X., Wang, S. X., Hao, J. M., Wang, L., Zhang, R., and An, Z.: Particle Size Distribution and Polycyclic Aromatic Hydrocarbons Emissions from Agricultural Crop Residue Burning, Environmental Science & Technology, 45, 5477-5482, 10.1021/es1037904, 2011.

Page 4: [1] Moved to page 4 (Move #1)	Microsoft Office User	7/1/20 10:30:00 PM

produced about 600 to 800 µg m^{-3} of mass loading in the chamber. The mass loading was estimated by determining the total aerosol volume, obtained by measuring the volume distribution with a scanning mobility particle sizer (SMPS) and assuming a density of
1 g cm^{-3} for fresh aerosol.

Page 5: [2] Deleted	Microsoft Office User	7/11/20 7:28:00 AM

MCE were calculated from CO and CO_2 measurements. These measurements underwent external calibration with either a pure gas (for CO_2) or a certified standard (199.7 ppm for CO and 5028 ppm for CO_2, purchased from Airgas National Welders). Gas filter correlation analyzers from Thermo Scientific were used to measure CO and CO_2 (models 48C and 41C, respectively). The change in the CO and CO_2 concentration was determined by comparing average measurements before a burn, and after the burn, once the measurements were stabilized. Averages of increase in concentration were taken soon after the measurements were stabilized, but before dilution could take place. Between 80s and 300s measurements at 10 Hz were averaged for the pre-burn state, and ~300s for the post-burn state. MCE was determined by the following equation:

$$MCE = \frac{\Delta[CO_2]}{\Delta[CO_2]+\Delta[CO]} \quad (1)$$

..

Page 7: [3] Deleted	Microsoft Office User	6/30/20 8:41:00 PM

2.1.3 Chamber cleaning

Between experiments, the smog chamber was flushed with zero air (from generator) for a minimum of 24 hours before starting the next experiment. The flow rate was varied somewhat but was at least 10 L min^{-1} up to usually no more than 20 L min^{-1}. The furnace was also cleaned during this time and was reconnected to the chamber while it is still flushing. Even when precautions were taken, this can introduce additional contaminants, which were also flushed out before a new burn. This additional flushing can take anywhere from 6 – 24 hours. When the chamber was not needed immediately, flushing continued at a constant 10 L min^{-1} to prevent room air from leaking into the chamber. Number concentrations were below 25 – 40 particles cm^{-3} as measured by the CPC before a new experiment began.

Page 11: [4] Deleted	Microsoft Office User	7/1/20 9:53:00 AM

It was found that, due to the presence of multiply charged particles, our reported SSA values were overestimated by a maximum of 8% for 200 nm and 300 nm particles.

The impact due to multiply charged particles is more significant for the higher temperature (flaming-dominated) burn than that of lower temperature (smoldering-dominated burn). The typical particle size distribution (corrected for multiple charging) of two different burning temperatures is shown in Figure S13.